

AD-A033 652

STANFORD RESEARCH INST MENLO PARK CALIF
INELASTIC COLLISIONS OF EXCITED ATOMS.(U)
NOV 76 K T GILLEN, T M MILLER, J R PETERSON
SRI-MP-76-105

F/G 20/8

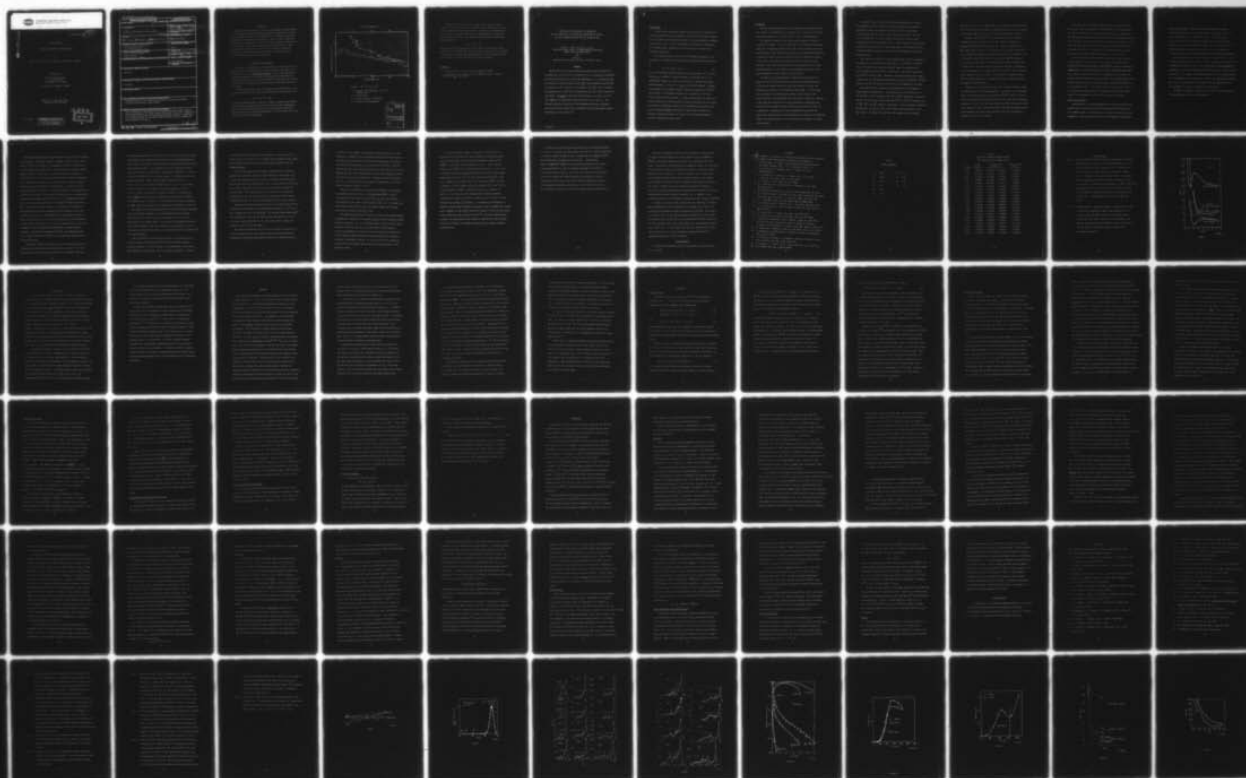
N00014-76-C-0118

UNCLASSIFIED

NL

1 OF 1
ADAO33652

TYPE



END

DATE
FILMED
2 - 77



STANFORD RESEARCH INSTITUTE
Menlo Park, California 94025 · U.S.A.

ADA033652

November 30, 1976

Annual Report

INELASTIC COLLISIONS OF EXCITED ATOMS

by

Keith T. Gillen, Thomas M. Miller, and James R. Peterson

Prepared for:

Office of Naval Research
Physics Branch
Washington, D.C. 20360

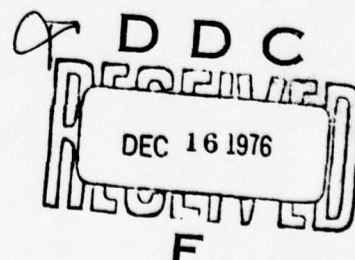
Attention: Dr. Doran W. Padgett

ONR Contract N00014-76-C-0118
SRI Project No. PYU-4529

#MP 76-105

DISTRIBUTION STATEMENT A

Approved for public release;
Distribution Unlimited



Unclassified

SECURITY CLASSIFICATION OF THIS PAGE (When Data Entered)

REPORT DOCUMENTATION PAGE		READ INSTRUCTIONS BEFORE COMPLETING FORM
1. REPORT NUMBER	2. GOVT ACCESSION NO.	3. RECIPIENT'S CATALOG NUMBER
4. TITLE (and Subtitle) INELASTIC COLLISIONS OF EXCITED ATOMS.		5. TYPE OF REPORT & PERIOD COVERED Annual Report, 1 Jul 75-30 Sep 76
7. AUTHOR(s) Keith T. Gillen, Thomas M. Miller, and James R. Peterson		6. PERFORMING ORG. REPORT NUMBER MP-76-105
9. PERFORMING ORGANIZATION NAME AND ADDRESS Stanford Research Institute 333 Ravenswood Avenue Menlo Park, California 94025		8. CONTRACT OR GRANT NUMBER(s) N00014-76-C-0118
11. CONTROLLING OFFICE NAME AND ADDRESS Office of Naval Research Physics Branch Washington, D.C. 20360		10. PROGRAM ELEMENT, PROJECT, TASK AREA & WORK UNIT NUMBERS 121103
14. MONITORING AGENCY NAME & ADDRESS (if different from Controlling Office)		12. REPORT DATE November 30, 1976
		13. NUMBER OF PAGES 3
		15. SECURITY CLASS. (of this report) Unclassified
		15a. DECLASSIFICATION/DOWNGRADING SCHEDULE
16. DISTRIBUTION STATEMENT (of this Report) Unlimited		
17. DISTRIBUTION STATEMENT (of the abstract entered in Block 20, if different from Report) Unlimited		
18. SUPPLEMENTARY NOTES		
19. KEY WORDS (Continue on reverse side if necessary and identify by block number) metastable atoms, atomic collisions, ionization, excitation transfer, collisional excitation, charge transfer		
20. ABSTRACT (Continue on reverse side if necessary and identify by block number) The interaction of metastable rare gas atoms with ground state atoms is being investigated in the energy range from several eV to 1 keV. Emphasis is on collisional ionization and collisional excitation transfer. Additional work examines details of the charge transfer reaction used to produce the fast metastable atom beams.		

DD FORM 1 JAN 73 1473

EDITION OF 1 NOV 65 IS OBSOLETE

Unclassified

SECURITY CLASSIFICATION OF THIS PAGE (When Data Entered)

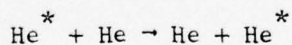
OBJECTIVES

Our work under this contract is aimed at improving the understanding of the fundamental mechanisms underlying gaseous excited state reactions. We are studying relatively simple systems that are amenable to detailed experimental and theoretical investigation. Some of these systems have direct practical application. Others are studied in order to predict the characteristics of more complicated systems by extrapolation. Understanding of these mechanisms is basic to any attempt to describe or anticipate the behavior of excited media such as visible and uv gas lasers, discharges, and excited atmospheres.

RESEARCH ACCOMPLISHMENTS

Some major accomplishments under this contract in the past year are detailed in the attached preprints of two papers that will appear in the February 1977 issue of The Physical Review A. These papers describe our detailed experimental and theoretical investigation of mechanisms for collisional ionization in the collision between a metastable and a ground state He atom. Collisional ionization work with other rare gas pairs is in progress.

In another experiment, still in progress, we are measuring the total excitation transfer cross section between metastable He and ground state He



at collision energies from ~ 10 -100 eV. Figure 1 compares these results with theoretical calculations of Evans and Lane¹ and with experimental results at higher energies obtained by a quite different technique.² Future plans call for a similar measurement of the ionization total cross section and its energy dependence.

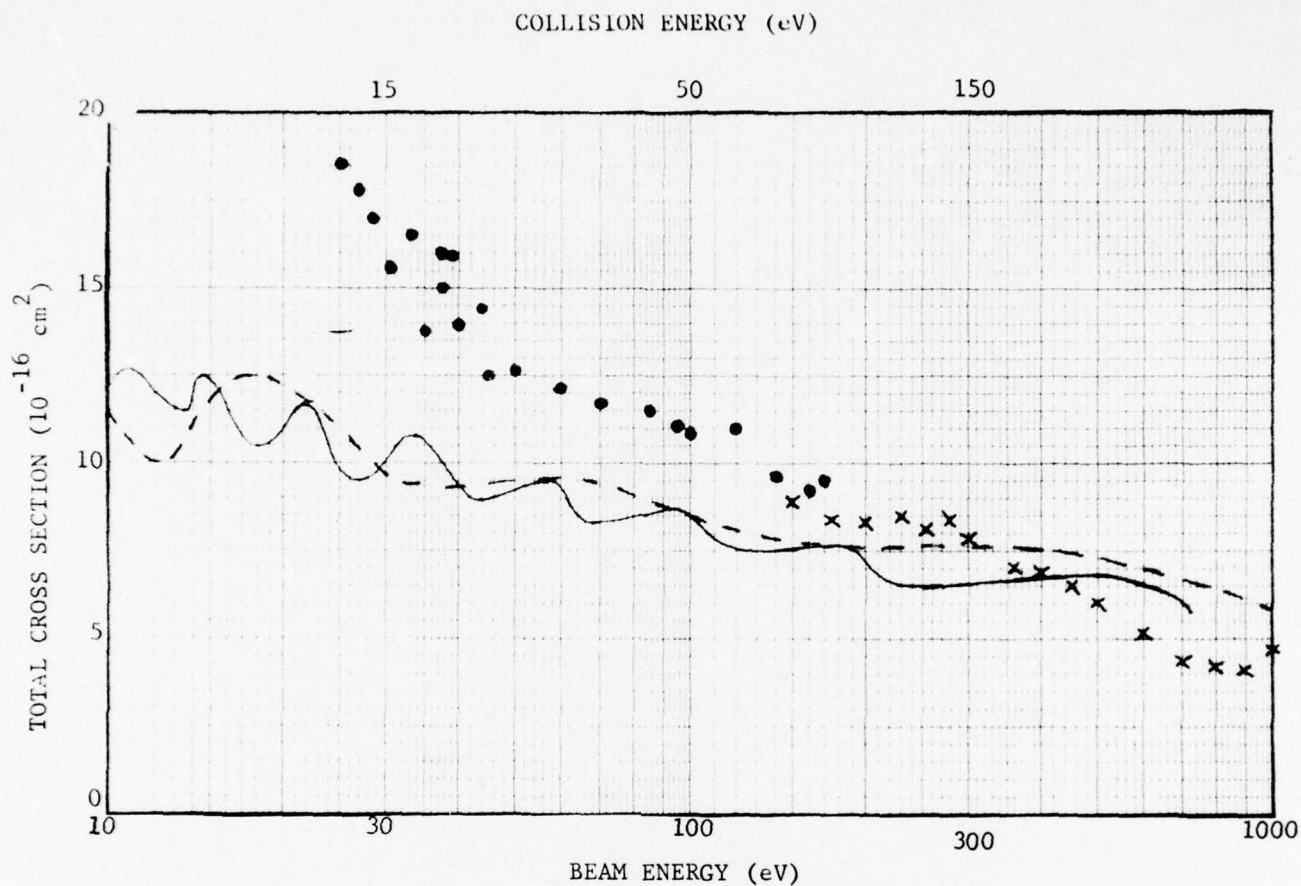


Figure 1. $\text{He}^* + \text{He} \rightarrow \text{He} + \text{He}^*$

× × × Earlier data (Hollstein, et al.² --
 $\text{He}(2^3\text{S})$ only)

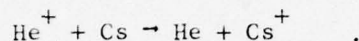
• • • Present data

--- Evans and Lane¹ (adiabatic)

— Evans and Lane¹(diabatic)

ADDITION for		
RTIS	White Section	<input checked="" type="checkbox"/>
DOC	Buff Section	<input type="checkbox"/>
UNANNOUNCED		<input type="checkbox"/>
JUSTIFICATION		
BY		
DISTRIBUTION/AVAILABILITY CODES		
DIST.	AVAIL.	ADD. OF SPECIAL
A		

A complementary aspect of our work under this contract involves studies of the very efficient near-resonant charge transfer process that is used to produce our fast excited beams. Theoretical calculations have been made (by R. E. Olson at SRI and E. J. Shipsey and J. C. Browne at the University of Texas) of the product state populations in the charge transfer reaction



The predicted product populations [60-70% ground state $\text{He}(1^1\text{S})$, 30-40% $\text{He}(2^3\text{S})$, and 1-2% $\text{He}(2^1\text{S})$ over the energy range 10-1000 eV] can be verified by experiments involving laser photoionization of the metastable excited beam particles. Work in this direction is being initiated.

References

1. S. A. Evans and N. F. Lane, Phys. Rev. 188, 268 (1969).
2. J. Hollstein, J. R. Sheridan, J. R. Peterson, and D. C. Lorents, Phys. Rev. 187, 118 (1969).

THEORETICAL INVESTIGATION OF A MECHANISM
FOR ION PRODUCTION IN COLLISIONS OF METASTABLE He WITH He:
AB INITIO POTENTIAL CURVES FOR $1\Sigma_g^+$ STATES OF He_2^+

Roberta P. Saxon and Keith T. Gillen
Molecular Physics Center, Stanford Research Institute,
Menlo Park, California 94025

and

Bowen Liu
IBM Research Laboratory, San Jose, California 95114

ABSTRACT

The mechanism of an observed ionization channel which produces He^+ at an energy loss of 18.7 ± 0.5 eV in 100-200 eV (c.m.) collisions of metastable He atoms with ground state He atoms was investigated. It is postulated that flux follows the diabatic singly excited $1\Sigma_g^+$ state associated with $\text{He}^*(2^1S)$ projectiles and then transfers to the doubly excited $1\Sigma_g^+$ state corresponding asymptotically to $2\text{He}^*(2^3S)$; autoionization follows at large internuclear separations. Ab initio calculations were performed on four He_2 states of $1\Sigma_g^+$ symmetry for internuclear separations of $0.72 a_0$ to $20.0 a_0$. The classical deflection function for the mechanism stated above, generated from the calculated potentials, is consistent with the experimental angular distribution of the product ions.

Introduction

A large amount of physical insight into the details of atom-atom and ion-atom interactions has been gained in the last ten years from a combination of theoretical and experimental work on scattering processes involving light atoms or ions.¹ Much of the progress has been due to improvements in the computational techniques that have been used to generate the interaction potentials.

In the preceding paper, Gillen et al.² describe measurements of the ionization of a 100-400 eV metastable He* beam colliding with ground state He



One of the ionization features observed at center of mass (c.m.) collision energies $E_{\text{cm}} = 100\text{-}200$ eV (labeled feature D) yields He⁺ ions at a cm translational energy loss of 18.7 ± 0.5 eV with an angular distribution peaking sharply at a value of $\tau = E_{\text{cm}} \theta_{\text{cm}} \approx 450 \pm 40$ eV-degrees. Although the metastable beam probably contains a much larger fraction of He*(2³S) than He*(2¹S),² no mechanism involving the 2³S component of the beam could be found to explain feature D. This paper postulates an ionization process involving the 2¹S projectiles as being responsible for this feature. We examine the requirements imposed by the experimental observations and verify, through ab initio calculations of interaction potentials and deflection function analysis, the ability of the proposed mechanism to match the experimental observations.

Background

The most important properties of the experimental collisional ionization feature to be understood are the energy loss of 18.7 ± 0.5 eV and the sharp angular peaking at a reduced angle $\tau = E\theta$ of ~ 450 eV-degrees.

The constraint imposed by the small angle threshold for process D is the most stringent. In order to lose 18.7 eV of relative translational energy, the interacting particles must climb a steep repulsive wall which would give much larger deflection angles than those observed experimentally. To explain low angle scattering, one must invoke an inelastic transition to an excited curve which is strongly attractive at relatively small distances. This attraction would deflect the trajectories back to small scattering angles in a way similar to that previously described for the major ionization channel³ (feature A) in this system.

As noted in the preceding paper,² energy loss values below 24 eV imply that the He^+ and He products are both in their ground electronic states and the excess energy loss above that necessary to ionize the metastable must reside in the outgoing electron energy. A fixed energy loss independent of scattering angle implies a fixed energy of the emitted electron. The postulated upper state with an inner well, required by low angle scattering, must be a He_2 intermediate autoionizing state since the 18.7 eV energy loss does not allow any excited He_2^+ states to be populated. Autoionization of this intermediate state yields the ground state products and an electron whose kinetic energy is the difference between the measured energy loss and the energy loss necessary to ionize the metastable.

The fixed energy of the ejected electron independent of scattering angle requires that the observed ionization takes place at internuclear separations R where the potential curves for the upper autoionizing molecular state and the final ion state are nearly parallel. This can most reasonably occur at large R where neither of the curves deviates significantly from its asymptotic limit. It also follows that the observed energy loss of 18.7 ± 0.5 eV is very nearly equal to the asymptotic energy difference between the initial state and the (intermediate) autoionizing molecular state.

The criterion of asymptotic energy difference may be used to determine the identity of the reactants and the products. The $\text{He}^*(2^3\text{S}) + \text{He}^*(2^3\text{S})$ limit, the lowest limit with two excited He atoms, is asymptotically 19.0 eV higher than the $\text{He}^*(2^1\text{S}) + \text{He}(1^1\text{S})$ limit and 19.8 eV higher than the $\text{He}^*(2^3\text{S}) + \text{He}(1^1\text{S})$ limit. Therefore, the observed energy loss strongly suggests that the intermediate autoionizing state has the $\text{He}^*(2^3\text{S}) + \text{He}^*(2^3\text{S})$ asymptote and that the initial reactant is the 2^1S component of the beam.

The identity of the molecular states involved may be determined by simple symmetry considerations. The two molecular states arising out of the $\text{He}^*(2^1\text{S}) + \text{He}(1^1\text{S})$ asymptote have $^1\Sigma_g^+$ and $^1\Sigma_u^+$ symmetries, respectively, whereas the three states arising from the $\text{He}^*(2^3\text{S}) + \text{He}^*(2^3\text{S})$ asymptote are of $^1\Sigma_g^+$, $^3\Sigma_u^+$, and $^5\Sigma_g^+$ symmetry, respectively. The only possible connection between these two sets of states is the radial coupling between the two $^1\Sigma_g^+$ states. It follows then that both the incoming and the outgoing

molecular states are of the $^1\Sigma_g^+$ symmetry. In addition, earlier consideration of the observed small angular threshold already has led us to conclude that the upper $^1\Sigma_g^+$ states must have a deep potential well at small R.

Previous calculations^{4,5} of the states of He_2 from the $2\text{He}^*(2^3\text{S})$ asymptote, chiefly by Garrison et al.⁵ only provided information at internuclear separations greater than $4 a_0$. Their calculation for the $^1\Sigma_g^+$ state showed a well of ~ 0.6 eV depth near $6 a_0$ and was repulsive at $4 a_0$. However, the existence of a short range well in the potential curve of the doubly excited $^1\Sigma_g^+$ diabatic state from the $2\text{He}^*(2^3\text{S})$ asymptote is at least consistent with the following simple chemical consideration. At large R the 2s orbitals interact attractively and this is responsible for the long range well. A barrier develops at smaller R due to electrostatic repulsion of the ion cores. At even smaller distances, however, there is strong bonding due to overlap of the core 1s orbitals and this may produce a deep inner well.

Therefore, all the experimental facts for ionization feature D might be consistent with the following mechanism. Analogously to the mechanisms found in the preceding paper, the reactants $\text{He}^*(2^1\text{S}) + \text{He}(1^1\text{S})$ initially follow the repulsive diabatic $^1\Sigma_g^+$ potential curve into small internuclear separation. In this case, they then cross to the $^1\Sigma_g^+$ doubly excited curve in the region of a deep inner potential well and depart to large distances with ionization taking place where the $\text{He}^* + \text{He}^*$ curve is essentially parallel to the $\text{He}^+ + \text{He}$ potential.

This model does not preclude ionization events at smaller R ; these events would yield a distribution of energy losses and scattering angles that may be too diffuse to be observed in the laboratory. Ionization at the turning point (minimum R) might be very intense, but escape observation due to deflection to large angles where the intensity is masked by a large number of other ionization processes involving the $\text{He}^*(2^3\text{S})$ or $\text{He}(1^1\text{S})$ components of the beam. In contrast, all ionization events at large R values would yield nearly identical energy loss values (19 eV).

We have therefore undertaken MCSCF calculations on four He_2 states of $1^1\Sigma_g^+$ symmetry, the ground state, two singly excited states and the doubly excited state dissociating to two $\text{He}^*(2^3\text{S})$ in order to look for the suggested well in the latter potential at small internuclear separations. The classical deflection function was then computed for the process in which the $\text{He}^*(2^1\text{S})$ metastable initially follows the incoming singly excited diabatic potential and then follows the doubly excited autoionizing state on the outgoing channel. The classical deflection function was found to be in qualitative agreement with the experimental observation, lending support to this explanation of the 18.7 eV energy loss process.

Method of Calculation

Approximations to the Born-Oppenheimer electronic wavefunctions and energies were calculated using the multi-configuration self-consistent field (MCSCF) method. The wavefunction of a desired electronic state was expanded in a limited N -particle basis set of orthonormal configuration

state functions (CSF). Each CSF was a linear combination of Slater determinants (SD) such that it had the symmetry and multiplicity of the desired electronic state. The SD's were built from an orthonormal one-particle basis set of symmetry and equivalence restricted spatial orbitals. The spatial orbitals were expanded in terms of a basis set of Slater-type functions centered at the atomic nuclei. The expansion coefficients, both N-particle and l-particle were determined variationally.

The He basis set used in our calculation is given in Table I. The 1s exponents are taken from the triple zeta basis of Clementi and Roetti.⁶ The 2s exponents of Garrison, et al.⁵ from a double zeta set was augmented by an exponent of 1.0, the hydrogenic value for Be 2s and 2p, the united atom limit of He_2 . The largest 2p exponent was chosen to give a maximum overlap with the dominant 1s basis function, $\zeta = 2.780$. The remaining 2p exponents were taken to evenly span the space between 4.17 and approximately .5. The hydrogenic Be 2p value is included by the procedure.

The MCSCF calculations included all CSF's that can be constructed by distributing four electrons in four orbitals:

$$\begin{array}{ll}
\text{ground state:} & 1\sigma_g^2 1\sigma_u^2 \\
\\
\text{singly excited:} & 1\sigma_g 1\sigma_u^2 2\sigma_g \\
& 1\sigma_g^2 1\sigma_u 2\sigma_u \\
\\
\text{doubly excited:} & 1\sigma_g^2 2\sigma_g^2 \\
& 1\sigma_g^2 2\sigma_u^2 \\
& 1\sigma_u^2 2\sigma_g^2 \\
& 1\sigma_u^2 2\sigma_u^2 \\
& 1\sigma_g 1\sigma_u ({}^1\Sigma_u^+) 2\sigma_g 2\sigma_u ({}^1\Sigma_u^+) \\
& 1\sigma_g 1\sigma_u ({}^3\Sigma_u^+) 2\sigma_g 2\sigma_u ({}^3\Sigma_u^+)
\end{array}$$

where the $1\sigma_g$ and $1\sigma_u$ orbitals correlate at the separated atom limit, with the $1s$ orbitals of He, and $2\sigma_g$ and $2\sigma_u$ with the $2s$ orbitals. The wave functions for the four lowest ${}^1\Sigma_g^+$ states, within the manifold of the configurations listed above, were determined in a single MCSCF calculation where a weighted average of the energies of the four states was minimized. Since we were chiefly interested in the features of the doubly excited state, the highest state was weighted more heavily than the others in our calculations. To avoid numerical difficulties caused by linearly dependent basis functions at small internuclear separation, the overlap matrix was diagonalized and all eigenvectors with eigenvalues less than 1×10^{-5} were excluded from our calculations. The MCSCF program developed by J. Hinze was used in these calculations.

Results and Discussion

Adiabatic potential curves for the singly and doubly excited $1\Sigma_g^+$ states of He_2 are shown in Fig. 1, while data for all states calculated are given in Table II. The ionic curve to which the assumed autoionization occurs is also indicated. The diabatic potentials are indicated by the dashed lines. It is clear from the figure that the avoided crossing between the highest two adiabatic states (or actual crossing of the diabatic states) near $1.5 a_0$ takes place over a rather narrow region. Examination of the coefficients of the CSF's in the wavefunctions shows that the crossing occurs between $1.4 a_0$ and $2.0 a_0$. Thus the description of the diabatic potential by simply drawing a smooth curve connecting points in the adiabatic non-crossing region was quite reasonable for our purposes here.

The doubly excited diabatic potential curve showed the expected inner attractive well at about $1.4 a_0$. It is bound by approximately 0.4 eV with respect to the two $\text{He}^*(2^3\text{S})$ asymptote and is approximately 4.0 eV lower than the hump in the potential curve at $2.5 a_0$. The potential also is attractive at long range, in this calculation being bound by about 0.13 eV around $7 a_0$. The calculation of Garrison, et al⁵ gave a depth for the outer well of 0.56 eV at an R_e of $6.34 a_0$. Since their calculation was designed to realistically represent long-range effects, while in the present work we were interested in describing the short-range, this discrepancy in the outer well was quite acceptable.

The singly excited states of He_2 , also shown in Fig. 1, may be observed to go through a rather broad crossing. Although $\text{He}^-(2^2\text{S})$ is not a stable species, $\text{He}^+(1^2\text{S}) + \text{He}^-(2^2\text{S})$ is the appropriate asymptotic designation of the other singly excited $^1\Sigma_g^+$ state, the first being the incoming channel, $\text{He}^*(2^1\text{S}) + \text{He}(1^1\text{S})$. These states have been calculated by Guberman and Goddard (GG)⁷ both in an adiabatic and fixed orbital (diabatic) representation. The diabatic results, given by the large dots in Fig. 1 smoothly connect the adiabatic potentials calculated here. The points have been translated upward by .05062 a.u. to bring the asymptote into agreement with the present calculation. Their adiabatic calculation had a well depth with respect to the asymptote of .644 eV at $R_e = 2.17 a_0$ compared with 1.18 eV at $R_e = 2.13 a_0$ for the present work. The singly and doubly excited He_2 $^1\Sigma_g^+$ states also have been included in a calculation by Gauyacq,⁸ but the incoming diabatic state appropriate to this experiment has not been estimated in that work. A calculation⁹ of the ground state and lowest doubly excited state of He_2 at very small internuclear distances produced a higher energy at $2.0 a_0$ than at $1.0 a_0$ for the upper adiabatic state, but the implication of a possible well at intermediate distances was not discussed. Another recent calculation¹⁰ using a very simplified model gave a diabatic doubly excited $^1\Sigma_g^+$ state in qualitative agreement with the present results.

The classical deflection function for a curve-crossing collision was calculated using the procedures outlined by Olson and Smith.¹¹ In this calculation the initial state was assumed to be the diabatic $^1\Sigma_g^+$ state

correlating asymptotically to $\text{He}^*(2^1\text{S}) + \text{He}(1^1\text{S})$ since the state correlating adiabatically to the reactants cannot interact with the outgoing molecular state except at very small R (Table II) and must therefore yield unacceptably large deflection angles. The outgoing state in the deflection function calculation was the autoionizing state correlating to $2\text{He}^*(2^3\text{S})$. To obtain the diabatic potential for the incoming channel, the following points were smoothly connected: values from the highest adiabatic state for $.75 a_0 < R < 1.4 a_0$ the second to highest for $1.5 a_0 < R < 2 a_0$ GG values at 2.6, 3.0 and $4.2 a_0$ and values for the third adiabatic state for $R > 4.5 a_0$, where the crossing was bridged as shown by the dashed line. The ab initio calculation gave the asymptotic separation of the incoming and outgoing states as 18.295 eV. For the deflection function calculation, the upper curve was translated to the spectroscopic separation of 19.023 eV.

The branch of the deflection function that yields the minimum scattering angle at each impact parameter is the one for which the particle goes adiabatically in its first transit of the crossing at $R \sim 1.5 a_0$ and diabatically in its second transit. That branch of the deflection function for a collision energy of 100 eV is plotted vs impact parameter in Fig. 2. The smallest scattering angle found in the deflection function is approximately 3.0° (300 eV-degrees).

From this minimum in the deflection function, the semiclassical Airy function analysis of Ford and Wheeler¹² was used to predict a quantum mechanical rainbow at $\tau \approx 490$ eV-degrees. The experimental cross section peaks sharply at 450 eV degrees and is in excellent agreement. At wider

scattering angles, other processes not considered in this paper also contribute to the 19 eV loss,² but the isolated feature peaking at small angles and an energy loss of 18.7 eV is certainly totally consistent with the assumed mechanism.

It may be noted that the calculation of Garrison et al.,⁵ which is expected to be the most reliable at large internuclear separations, had an outer well approximately 0.56 eV deep. If molecular ionization takes place in this outer well region rather than at larger distances, the energy loss could be lower than the asymptotic 19.0 eV value by the amount of the well depth. The measured energy loss of 18.7 ± 0.5 eV allows this possibility, and the deflection function for this process would deviate insignificantly from the case where ionization occurs at larger distances.

Long range molecular autoionization from the same doubly excited state discussed here has, however, also been observed by Gerber et al.,¹³ in the case of ground state He + He collisions. The electron energy distribution¹⁴ for autoionization from this same $1\Sigma_g^+$ excited state peaks at 15.0 eV at a collision energy comparable to ours; this would imply an energy loss peaking at 19.0 eV in our experiment.

The present experimental data by no means precludes the existence of intense ionization at the turning point since that process would yield scattering at wide angles which would be difficult to resolve from other

channels; but the evidence of long range autoionization cannot be taken lightly as it suggests that an observable fraction of the doubly-excited reactants escape from small R without having autoionized. This result also predicts the observation of scattered neutral $\text{He}^*(2^3\text{S}) + \text{He}^*(2^3\text{S})$ products with the same angular distribution and energy loss as that of the observed He^+ ions since autoionization at large R also undoubtedly takes place with less than unit probability. A similar prediction for ground state $\text{He} + \text{He}$ collisions has been confirmed by Morgenstern et al.¹⁵ and studied in detail by Brenot et al.¹⁶

Finally, it is desirable to estimate the probability for following the postulated potential curves. The approaching $\text{He}^*(2^1\text{S}) + \text{He}(1^1\text{S})$ reactants must first follow a diabatic $^1\Sigma_g^+$ curve into the continuum, transferring from the lowest excited adiabatic $^1\Sigma_g^+$ curve to a higher one, then proceed adiabatically in the first passage through the crossing region with the doubly excited $^1\Sigma_g^+$ curve.

The Landau-Zener theory may be applied in this latter crossing region, estimating the strength of the diabatic coupling from the splitting between adiabatic potentials. At a c.m. collision energy of 100 eV and for impact parameters between $0.9 a_0$ and $1.3 a_0$, the region of the deflection function corresponding to the peak in the cross section, the probability for an adiabatic passage through this crossing region on the incoming trajectory lies between 5 and 20%. It is then clear that a significant fraction of the trajectories which reach this crossing continue in the postulated manner.

It is more difficult, however, to estimate the fraction of the original flux which reaches this upper crossing by passing diabatically through crossings with states arising from asymptotes lower than the $2\text{He}^*(2^3\text{S})$. Such states are not indicated in Fig. 1. One may make an analogy to the $\text{He}^*(2^3\text{S}) + \text{He}$ collision studied previously.³ In that case an estimate of diabatic passage was based on the two-state close-coupled computations of Evans et al.¹⁷ for the transition probabilities at the first crossing of the diabatic $^3\Sigma_g^+$ curve (leading to $\text{He}^*(2^3\text{S}) \rightarrow \text{He}(2^3\text{P})$ excitation). From the smaller gap in the analogous $^1\Sigma_g^+$ curves⁷ (at the crossing leading to $\text{He}^*(2^1\text{S}) \rightarrow \text{He}(2^1\text{P})$ excitation), one estimates at 100 eV c.m. the fraction of 2^1S collisions which initially proceed diabatically is probably substantial, perhaps as much as 30-40 % of those following the incoming $^1\Sigma_g^+$ potential. In estimating the probability of diabatic passage through subsequent crossings, it may be assumed that coupling matrix elements for the singlet manifold are similar to those for the triplet states, which have been calculated by Cohen.¹⁸ From these triplet matrix elements, the Landau-Zener theory predicts a probability of 80% for going diabatically through all subsequent crossings for the impact parameters considered here.

The above result has interesting implications for the energy dependence of feature D. At higher collision energies than 100 eV, a smaller probability of adiabatic passage through the final crossing with the outgoing $2\text{He}^*(2^3\text{S})$ state would tend to decrease the cross section. This fraction might be compensated somewhat by an increase with energy in the fraction proceeding diabatically into the continuum, although that fraction is already quite large at 100 eV. Since the total ionization cross sections for both the singlet and triplet metastables are expected to increase substantially with energy as the initial diabatic probability increases, the fractional contribution from process D to the total cross section may be expected to decrease as the relative energy increases beyond 100 eV.

No direct experimental comparison of the intensity of feature D with the other ionization channels can be made, since the ratio of $\text{He}^*(2^1\text{S})$ to $\text{He}^*(2^3\text{S})$ in the beam is unknown and may even vary considerably with beam energy. Nevertheless, the expected energy dependence leads to the conclusion that this channel might be more difficult to observe at collision energies higher than those studied here. This is especially true in measurements of the emitted electron energy, where electrons produced at the turning point (process B²) yield an intense continuum electron energy distribution. Any attempt to measure the 15 eV electrons from process D through the interfering continuum should emphasize procedures that minimize the relative contribution from other ionization channels, e.g., by working at low collision energies and by attempting to maximize the beam fraction of $\text{He}^*(2^1\text{S})$.

In summary, the calculations reported here were undertaken to investigate the mechanism of He^+ ion production at an energy loss of 18.7 eV in collisions of metastable He atoms with ground state He atoms. The results are consistent with the postulated ionization mechanism that flux follows the diabatic singly excited $1\Sigma_g^+$ state associated with $\text{He}^*(2^1\text{S})$ projectiles and then transfers to the doubly excited $1\Sigma_g^+$ state corresponding asymptotically to $2\text{He}^*(2^3\text{S})$. It also appears that molecular autoionization occurs from the latter state at large internuclear separations where it is essentially parallel to the He_2^+ potential.

ACKNOWLEDGEMENT

We gratefully acknowledge the usual enlightening conversations with Dr. R. E. Olson.

REFERENCES

✓ APS supported by Atmospheric Sciences Section, National Science Foundation Grant ATM-74-23738; KTG supported by Office of Naval Research.

1. See for example: M. Barat, Invited Lectures and Progress Reports, VII ICPEAC, Beograd, 1973, P. 43, R. McCarroll, *ibid*, p. 71.
2. K. T. Gillen, J. R. Peterson, and R. E. Olson, *Phys. Rev.* (preceding paper).
3. K. T. Gillen, D. C. Lorents, R. E. Olson, and J. R. Peterson, *J. Phys. B: Atom. Molec. Phys.* 7, L327 (1974).
4. D. J. Klein, *J. Chem. Phys.* 50, 5151 (1969).
5. B. J. Garrison, W. H. Miller, and H. F. Schaefer, *J. Chem. Phys.* 59, 3193 (1973).
6. E. Clementi and C. Roetti, *At. Data Nucl. Data Tables* 14, 177 (1974).
7. S. L. Guberman and W. A. Goddard III, *Chem. Phys. Letters* 14, 460 (1972); *Phys. Rev. A* 12, 1203 (1975). S. Guberman, thesis, Cal Tech, 1972.
8. J. P. Gauyacq, *J. Phys. B: Atom. Molec. Phys.* 9, 2289 (1976).
9. D. R. Yarkony and H. F. Schaefer III, *J. Chem. Phys.* 61, 4921 (1974).
10. T. M. Kereselidze, *Sov. Phys. JETP* 42, 33 (1976) [*Zh. Eksp. Teor. Fiz.* 69, 67 (1975)].
11. R. E. Olson and F. T. Smith, *Phys. Rev. A* 3, 1607 (1971).
12. K. W. Ford and J. A. Wheeler, *Ann. Phys. (N.Y.)* 1, 259 (1959).
13. G. Gerber, R. Morgenstern, and A. Niehaus, *J. Phys. B: Atom. Molec. Phys.* 6, 493 (1973); see also M. Barat, D. Dhuicq, R. Francois, C. Lesech, and R. McCarroll, *J. Phys. B: Atom. Mol. Phys.* 6, 1206 (1973).
14. G. Gerber and A. Niehaus, *J. Phys. B: Atom. Molec. Phys.* 9, 123 (1976).
15. R. Morgenstern, M. Barat, and D. C. Lorents, *J. Phys. B: Atom. Molec. Phys.* 6, L330 (1973).
16. J. C. Brenot, D. Dhuicq, J. P. Gauyacq, J. Pommier, V. Sidis, M. Barat, and E. Pollack, *Phys. Rev. A* 11, 1245 (1975).
17. S. A. Evans, J. S. Cohen, and N. F. Lane, *Phys. Rev. A* 4, 2235 (1971).
18. J. S. Cohen, *Phys. Rev. A* 13, 86 (1976).

Table I

ORBITAL EXPONENTS

1s	4.346	2p	4.17
1s	2.780	2p	2.09
1s	1.453	2p	1.04
2s	1.0	2p	.52
2s	.65		
2s	.46		

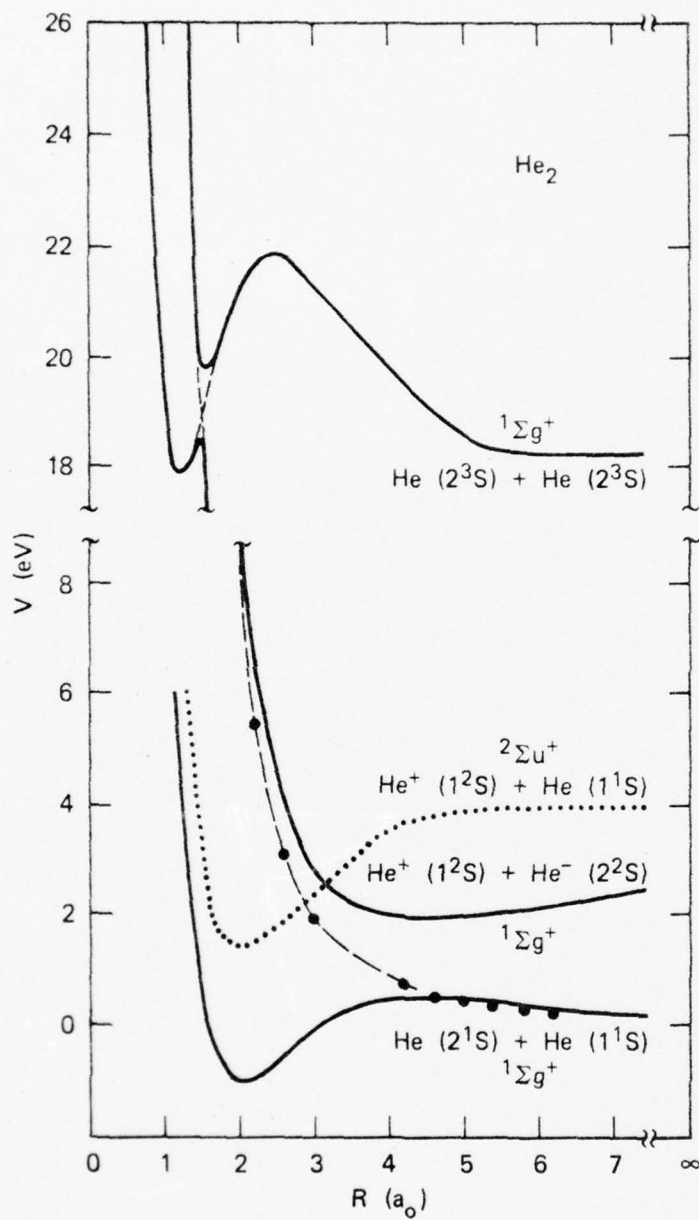
Table II
CALCULATED POTENTIAL CURVES FOR FOUR
 $1\Sigma_g^+$ STATES OF He_2 IN ATOMIC UNITS

$R \text{ (a}_0\text{)}$	Ground State	Singly-excited States		Doubly-excited state
0.75	-4.105283	-4.027943	-3.970071	-2.177459
0.80	-4.263832	-4.177596	-4.073123	-2.442453
1.00	-4.735469	-4.579067	-4.275862	-3.241114
1.15	-4.978981	-4.754282	-4.313941	-3.653895
1.25	-5.106667	-4.833966	-4.314419	-3.868054
1.35	-5.212513	-4.892529	-4.304558	-4.044137
1.40	-5.258314	-4.915601	-4.297587	-4.119744
1.50	-5.337807	-4.951567	-4.290011	-4.241862
1.75	-5.480107	-4.999543	-4.498044	-4.226374
2.00	-5.566201	-5.012056	-4.649280	-4.189862
2.50	-5.648266	-4.996064	-4.807032	-4.167825
3.00	-5.677560	-4.972506	-4.869955	-4.187746
3.50	-5.687938	-4.959292	-4.891901	-4.217097
4.00	-5.691368	-4.953899	-4.891901	-4.217097
4.50	-5.692148	-4.952413	-4.899824	-4.269326
5.00	-5.691904	-4.953612	-4.898843	-4.285788
6.00	-5.690849	-4.958575	-4.893131	-4.300947
7.00	-5.690111	-4.962788	-4.885073	-4.303330
8.00	-5.689939	-4.966215	-4.874653	-4.302298
10.00	-5.690146	-4.969825	-4.855172	-4.300442
20.00	-5.690028	-4.970835	-4.812138	-4.298498

FIGURE CAPTIONS

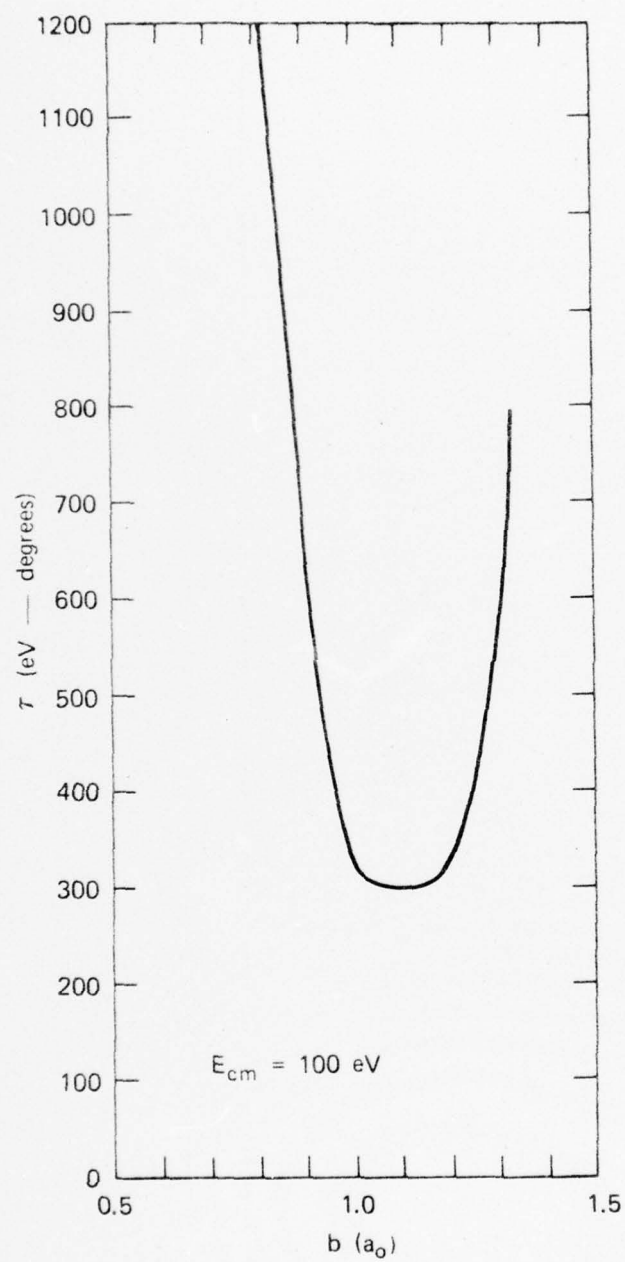
Fig. 1. Adiabatic $\text{He}_2 \ ^1\Sigma_g^+$ potential curves calculated here are plotted with solid lines. Top curve is the doubly excited state. The other two curves are singly excited states. The ground state has been omitted. Diabatic states are indicated by dashed lines. The points of Guberman and Goddard (Ref. 7) translated to agree asymptotically with the present calculation are given by large dots. The dotted curve approximates the $^2\Sigma_u^+$ state of He_2^+ . Although $\text{He}^-(2^2S)$ is not a stable species, $\text{He}^+(1^2S) + \text{He}^-(2^2S)$ is the appropriate asymptotic designation of the higher singly excited state. Asymptotically it lies above the $^2\Sigma_u^+ \text{He}_2^+$ state.

Fig. 2. Reduced classical deflection function $\tau = E_{\text{cm}} \theta$ (where θ is the c.m. deflection angle) plotted versus impact parameter b for a collision where the initial channel is the diabatic state correlating to $\text{He}^*(2^1S) + \text{He}(1^1S)$, the final channel is the diabatic state correlating to $2\text{He}^*(2^3S)$, and the flux transfers from the initial to the final channel the first time it traverses the crossing.



SA-4005-3R

FIGURE 1



SA-4005-4

FIGURE 2

IONIZATION IN COLLISIONS OF METASTABLE He WITH He⁺

Keith T. Gillen, James R. Peterson, and Ronald E. Olson
Molecular Physics Center
Stanford Research Institute, Menlo Park, California 94025

ABSTRACT

Detailed differential cross section measurements have been performed for production of He⁺ in collisions of metastable He*(2³S and 2¹S) with He at center-of-mass energies of 50, 99, and 199 eV. The product ion distribution contains several distinct features dominated by an intense peak at small angles and an energy loss value near threshold. The major features of the ionization are shown to be consistent with various calculated processes, each of which follows the Σ_g^+ diabatic repulsive potential on the incoming trajectory. Ionization occurs at the crossing into the continuum, at the classical inner turning point, at crossings with higher continua, and through molecular autoionization of doubly-excited neutral states. Possible contributions from He⁺ + He⁻ auto-ionizing states are considered. Evidence is found for significant contributions to the ionization from the small amount of He*(2¹S) in the beam.

INTRODUCTION

The He_2 system is an ideal choice for the study of collisional processes because it is simple enough that accurate theoretical calculations can be compared with most experimental results. The interaction potentials can be obtained using ab initio techniques and the dynamical properties can be deduced from trajectory calculations on the relevant potential curves using estimates of the couplings between curves near crossings or avoided crossings. One of the important problems remaining to be understood in collision physics is the nature of the coupling between a discrete state and a continuum. Little detailed data exist for comparison with theory. Collisional ionization experiments in simple systems should contribute significantly to the understanding of the general problem, since the discrete state interactions are well enough understood that effort can be concentrated on the continuum coupling mechanisms.

In this paper we present a detailed study of collisional ionization in the scattering of a beam of metastable helium by helium target gas in the center-of-mass (c.m.) energy range 50-199 eV. Several ionization channels are identified by demonstrating that the deflection functions and energy losses calculated on the pertinent potential curves are consistent with the experimental results. A companion paper describes the calculation of the potential energy curves for the $^1\Sigma_g^+$ states of He_2 , and demonstrates their relevance to one of the prominent ionization channels.

This experiment represents the first measurement of the collisional ionization of metastable He at low energies and contains the first detailed analysis of the product ion angle-energy distribution. In a preliminary publication we described the most intense feature of the collisional ionization.¹

Several recent studies of ground state rare gas collisions in the energy range from several hundred to several thousand eV have examined the details of various ionization processes either by measurements of the emitted electron energies^{2,3} or of the product ion energy-angle distributions.⁴⁻⁷ The ionization is associated with intimate encounters where the incoming ground state potential is generally thought to couple at small internuclear distances, high on the repulsive wall, to excited discrete levels which cross into the continuum and autoionize on the outgoing portion of the trajectory. All of the ionization channels identified have large angular thresholds dictated by the significant repulsive forces at short distances. In contrast, the major ionization channels observed in the present investigation have much smaller angular thresholds than anticipated from a first consideration of the interaction potentials.

APPARATUS

The metastable differential scattering apparatus has been described in detail previously.⁸ A beam of fast He^+ ions enters a charge exchange cell filled with Cs. Near-resonant charge transfer produces He atoms predominantly in the 1^1S , 2^1S , 2^1P , 2^3S and 2^3P states, and radiation of the P states leaves a fast neutral beam composed of excited metastable 2^1S , 2^3S , and ground state 1^1S He. The composition of the resulting neutral beam has been estimated theoretically by Olson, Shipsey, and Browne⁹ using ab initio potential energy curves and close-coupling calculations. They find that the charge transfer He beam contains 30-35% 2^3S , less than 1% 2^1S , and 65-70% 1^1S in the energy range from 200-400 eV. At lower collision energies, these theoretical calculations are in agreement with experimental evidence^{8,10,11} that there is indeed a large ratio of 2^3S to 2^1S metastables. The He^+ ions that do not undergo charge transfer are deflected out of the beam before the fast neutrals enter a scattering cell filled with He at pressures low enough to insure single collision conditions. Scattered particles are detected by two channeltron detectors that can be rotated around the scattering cell. One detector (A) measures the total scattered product intensity as a function of angle and detects both ionic and neutral particles; deflectors between the scattering cell and the detector can remove the ions so that only neutrals are counted, allowing a determination of ionic and neutral

product angular distributions separately. The other detector (B) is mounted behind a 127° energy analyzer and can measure the angle-energy double-differential cross section for product ions.

A large exit slot in the target cell allows both detectors, when positioned within the laboratory angular range $+75^\circ$ to -25° , to view the entire intersection of the beam with the target cell. Collimators in front of detector A are used to shield it from background contributions without blocking its view of the interaction region. A collimator at the entrance to the 127° analyzer limits and defines the acceptance solid angle from every position in the interaction region. Both detectors accept a constant solid angle range from every location in the interaction region independent of the angular location of the detector. Hence, there is no "viewing factor" correction needed in comparing the measured intensity at different scattering angles.

Electrostatic deflectors can be used to pulse the original ion beam before it enters the alkali charge transfer cell. By measuring the difference in flight time to detector A between the original ion beam and the metastable beam and using a separate determination of the ion beam energy with detector B, one can determine the energy of the neutral beam with an accuracy of approximately 0.5 eV. The neutral beam has a lower energy than the parent ions, due mostly to the contact potential of the Cs covered surfaces in the charge transfer oven.

For analyzing scattered product ion energies, the 127° analyzer is set to transmit a specific ion energy (119 eV in the experiments reported here) with a fixed resolution (measured to be 2.6% [3.1 eV] full width at half maximum, FWHM). A few experiments were done with higher energy resolution, but no additional structure (beyond that reported here) was resolved. Energy scanning is achieved by varying the potential of the entire energy analyzer system. Most of the scattering data were obtained by scanning the product ion energy at a fixed beam energy and laboratory scattering angle. In a typical experiment, a product energy is selected and ions are counted for a specified length of time (e.g., 30 seconds). These detected ions include a background produced by collisions of beam metastables with target gas streaming from the scattering cell. By admitting He gas to the main chamber at the same rate that it was previously admitted to the scattering cell, we can determine the background contribution. The floating potential is then varied stepwise to measure both the signal and the background at other product energies. The first point is remeasured occasionally during the course of a scan as a check for variations in beam intensity or scattering gas pressure.

The retardation associated with the floating energy analyzer would be expected to partially defocus the product ions, thereby lowering the counting rate. We compensate for this by a lens in front of the analyzer, adjusted for maximum transmission of the ions with energies

corresponding to the peak of the product distribution. The lens voltages were then held constant relative to the analyzer floating voltage. Variations in collection efficiency for ions of different energy have been shown to be small over the energy range of each of the scans presented here. Refocussing the lenses for maximum transmission at every energy in a scan did not increase the intensity at any energy by more than 10% relative to measurements made with constant lens voltages.

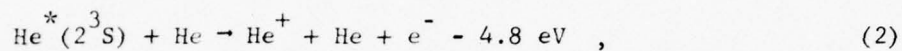
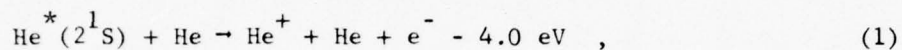
In the plane of motion of detector B, the detector angular resolution is calculated to be 0.3° FWHM; the beam profile has a comparable angular width. The angular acceptance perpendicular to the plane of motion of the detector is $\pm 0.5^\circ$ FW. This out-of-plane window allows scattered particles of larger angle than the nominal apparatus setting to be collected, but the average effect is insignificant at nominal scattering angles beyond $\sim 1^\circ$.

Another source of angular broadening, increasing monotonically with scattering angle but significant only at wide angles, is due to the detector's view of the entire scattering volume 1 mm dia. by 1.25 cm length. At a laboratory angle of 10° , scattering from the entrance and exit regions of the scattering cell is at angles 9.3° and 10.7° , respectively. This broadening does not affect any of the conclusions drawn from the data, although it might decrease the detail observable at the larger scattering angles.

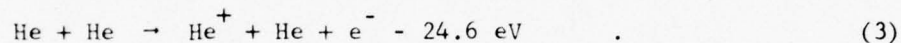
EXPERIMENTS

General Remarks

The neutral He beam is a mixture of 2^1S and 2^3S metastables and 1^1S ground state. The least endothermic collisional ionization channels for the three components are, respectively,



and



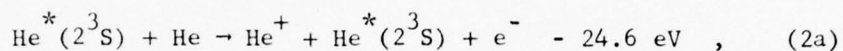
The endothermicities given are for ionization at threshold with ground state products. For each reaction, the electron can also be ejected with nonzero energy and the product He and He^+ can be formed in excited electronic states.

Figure 1 presents a kinematic diagram and defines some of the symbols to be used in this paper. For product particles of equal mass (neglecting the mass of the electron), an ion detected at laboratory coordinates E', θ_L will correspond to a translational energy loss in the c.m. system of

$$\Delta E \equiv E_{\text{cm}} - E'_{\text{cm}} = 2(E' E_0)^{\frac{1}{2}} \cos \theta_L - 2E' . \quad (4)$$

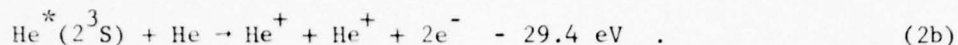
It is evident that the measured ΔE must equal the sum of the emitted electron energy and the change in internal energy of the heavy particles.

Consider reactions of $\text{He}^*(2^3\text{S})$ as an example. The internal energy of $\text{He}^*(2^3\text{S})$ is 4.8 eV less than the amount required to produce ionic products. Therefore 4.8 eV is the minimum ΔE required to produce ions from reaction (2) and would correspond to zero energy electrons and ground state products. The first electronically excited product channel is



accessible only with measured ΔE values of at least 24.6 eV. Therefore, for ΔE values less than 24.6 eV reaction (2a) is not possible, and only ground state products are allowed. If $4.8 \text{ eV} < \Delta E < 24.6 \text{ eV}$, the additional endothermicity $\Delta E - 4.8 \text{ eV}$ must reside in kinetic energy E_e of the departing electron. Assuming a pure $\text{He}^*(2^3\text{S})$ beam, there is no ambiguity in product states or electron energies for measured ΔE values in this range. For $\Delta E = 24.6 \text{ eV}$, reactions (2) and (2a) are both possible, giving 19.8 eV energy either to neutral He product excitation or to the electron translational energy. At higher ΔE values, the entire manifold of He excited

states becomes energetically accessible with a limit at



Ionization of the ground state component of the beam [Reaction (3)] is another possible channel at $\Delta E \geq 24.6 \text{ eV}$. However, the contributions from (3) can be estimated from the ions produced by scattering a pure beam of ground state He from a He target. Replacing the Cs charge transfer vapor with He gas allows resonant charge transfer production of fast He ground state beams for these measurements. Data^{4,5} for reaction (3) exist at slightly higher energies than our measurements and a comparison of energy loss profiles can be made.

Although the ratio of $\text{He}^*(2^3\text{S})$ to $\text{He}^*(2^1\text{S})$ in the metastable beam is thought to be large,⁸⁻¹¹ contributions from a small component of $\text{He}^*(2^1\text{S})$ might dominate at some values of product energy transfer and scattering angle if the important ionization processes for the two metastables are quite different. Even if the mechanisms were similar for both metastables, the threshold for $\text{He}^*(2^1\text{S})$ ionization might appear at a lower energy because the singlet state is energetically closer to the ionization limit. Since the energetics of reactions (1) and (2) are only 0.8 eV different, the estimated 0.5 eV uncertainty in beam energy makes it unlikely that the effects of the two metastable reactants can be separated upon a first examination of the data. For convenience, we will initially analyze the scattering in terms of the larger 2^3S component of the beam; however, contributions from 2^1S will also be discussed.

Energy Distributions

Figure 2 shows an example of a product He^+ ion energy distribution. The data at a metastable beam energy $E_0 = 100.2$ eV and a laboratory scattering angle $\theta_L = 0.0^\circ$ present the measured He^+ distribution plotted vs. the laboratory energy E' . In this spectrum, a single feature is observed with a c.m. energy loss ΔE of 4.5 eV. The 0.5 eV uncertainty in beam energy implies that the He^+ ions can be from either reaction (1) or (2) or both; for either reaction, the products are in their ground electronic states and the electron energy is small (< 1 eV). There can be no contribution to this feature from ionization of ground state He in the beam.

The measured energy width of this peak, $\text{FWHM} = 3.6$ eV, is a convolution of the beam energy width, the width due to the distribution of product electron energies, and the width associated with the energy analyzer. The energy analyzer FWHM of 2.6% is 3.1 eV at the 119 eV analysis energy. Hence, the removal of the detector broadening would lower the FWHM to $\sim (3.6^2 - 3.1^2)^{1/2} = 1.8$ eV. The energy width of the original metastable beam is not as easy to ascertain. The beam energy was measured by a time-of-flight (TOF) technique involving a pulsed electric field deflection of the original He^+ ion beam before it was converted by charge transfer to a neutral beam. One major problem with TOF measurement of beam energy

width is associated with contributions from the various components of the beam. Each of the He charge transfer products 1^1S , 2^1S , 2^1P , 2^3S , and 2^3P has a different energy defect and produces fast neutrals of slightly different energy. The 2^1P component radiates to become ground state He(1^1S) which can contribute to the apparent beam energy width but does not contribute to the scattered ion peak in Fig. 2. The same argument holds for He(1^1S) formed directly by charge transfer reactions that yield excited Cs⁺ states. The amount of broadening (and shifting) of the measured beam energy due to this component depends on its relative amount and also on whether He(2^3S)^{*} is formed directly or through radiation from He(2^3P). In addition, the act of pulsing the beam can perturb its measured energy distribution from the unpulsed value, usually broadening it somewhat. The result is that the "measured" widths of the neutral beam were variable and usually larger than the 1.8 eV upper limit. Hence, the true energy profile of the metastable beam cannot be obtained from the TOF measurements.

Obviously the ion beam energy width can be used as a lower limit for that of the metastable beam. Measurements with the energy analyzer suggest a width of ~ 1.0 eV for the parent ion beam. Then the energy width of the emitted electron distribution could be as much as $\sim (1.8^2 - 1.0^2)^{\frac{1}{2}} = 1.5$ eV, but is probably smaller. The uncertainty in beam energy width precludes any serious attempt at deconvoluting the measured energy profiles, but the 3.1 eV FWHM of the 127^o energy analyzer is the major source of energy broadening. One can still conclude that the ions observed (Fig. 2)

correspond to low energy (< 1 eV) electrons having a small (< 1.5 eV) spread in energy.

Figure 3 shows representative collisional ionization data at a c.m. energy $E_{cm} = 99$ eV ($E_o \approx 198$ eV). The intensity scale is arbitrary; but the various curves have been normalized to each other by an angular scan that compares the peak intensity from one angle to the next. The data are presented in the laboratory frame without any deconvolution; the measured intensity is proportional to $\frac{d^2\sigma}{d\Omega dE}$, where $d\Omega$ is a differential laboratory solid angle element. Various values of the c.m. energy loss, ΔE , calculated from Eq. (4) have been indicated on the figure. At every angle the energy loss profile is dominated by a peak at $\Delta E \approx 5.0$ eV. This component of the He^+ product distribution is labelled "A" and will be discussed below. Other prominent features are designated B, C, and D and will also each be described in terms of specific excitation mechanisms. Unlabelled features at large energy loss values and large angles can have several causes and will only be mentioned briefly.

Figure 4 shows similar representative data at a c.m. energy $E_{cm} = 199$ eV ($E_o \approx 398$ eV). As in Figure 3, the intensities are normalized to unity at the peak of the distribution ($\theta_L = 0.0^\circ$, $\Delta E = 5$ eV), and prominent features are labelled for subsequent discussion. The distributions at angles smaller than 1.0° (not shown in Fig. 4) are quite similar at the same value of $\tau = E_o \theta_L$ to the corresponding small angle data at the lower collision energy, although the feature labelled "D" is less prominent than it is in Fig. 3.

At 50 eV c.m. energy the scattered signal is significantly smaller than at the higher energies, which causes difficulty in observing any more than the most prominent features. Energy scans at laboratory angles of 0° (Fig. 2) and 1.2° show only feature "A" with an energy loss peaking at $\Delta E = 4.5$ eV; for angular scans at a fixed $\Delta E = 4.5$ eV, it was possible to follow this feature out to $\sim 5^\circ$ before it became comparable in size to the background noise.

The laboratory data can be converted to corresponding c.m. differential cross sections through the transformation

$$\frac{d^2\sigma}{d\omega dE'_{cm}} = \frac{w'}{v'} \frac{d^2\sigma}{d\Omega dE'} , \quad (5)$$

where $d\omega$ is the c.m. solid angle volume element, E'_{cm} is the product relative translational energy, and $\frac{w'}{v'}$ can be determined using

$$\frac{w'}{v'} = \left(\frac{E'_{cm}}{2E'} \right)^{\frac{1}{2}} = \left(\frac{[E_{cm} - \Delta E]}{2E'} \right)^{\frac{1}{2}} \quad (6)$$

and Eq. (4). For the small scattering angles and relatively small energy losses evident in the data considered here, the Jacobian of transformation $\left(\frac{w'}{v'} \right)$ varies by little more than 10% over the entire range of data. Transformation to the c.m. would, for example, decrease the intensity of feature C in Figure 3 by only about 6% relative to peak A. These changes are comparable to estimates of the uncertainty in peak ratios associated with the energy scanning method used in these experiments (see "Apparatus"), and the two effects should partially compensate.

The c.m. distributions will not be shown directly due to problems associated with presenting the data in that format. As is evident from the kinematics, a particular laboratory angle does not map into a single c.m. angle. Hence, c.m. energy loss distributions at specified angles must be obtained by interpolation of laboratory data, or the c.m. data must be presented as an energy-angle contour map of product intensity. In either case, the large variation in product intensity ($> 10^4$) implies that a significantly larger set of data would be needed to produce and to present c.m. results with the clarity of detail possible in Figures 3 and 4. The existing data are adequate for extracting the essential aspects of the primary ionization processes observed without transforming to the c.m. A rough estimate of the c.m. scattering angle θ_{cm} is its lower limit

$$\theta_{cm} \approx 2\theta_L \quad (7)$$

A more accurate formula for determining θ_{cm} ,

$$\sin\theta_{cm} = \left(\frac{v'}{w}\right) \sin\theta_L \quad (8)$$

involves the same conversion factor used in Eq. (5) for relating laboratory and c.m. differential cross sections. Again for the low angle scattering and small energy losses measured here, the range in $\left(\frac{v'}{w}\right)$ is small; in Figure 3, θ_{cm} would be $\sim 1\%$ and 8% higher than the estimate of Eq. (7) for peaks A and C, respectively, at all angles.

Angular Distributions

The angular normalizations referred to above involve measurements of the angular distribution of a specific feature by adjustment of the analysis energy to transmit the peak of the feature at every angle. Our preliminary report¹ on this work presented angular normalization data for peak A at all three collision energies studied. Those distributions (shown in Fig. 5) were used to normalize energy distributions from one angle to another. The angular distributions for all of the other major ionization features are more difficult to determine, since there is only a limited range of angles for which each feature is clearly resolved from other channels. Figure 6 shows an angular normalization for feature C at $E_{cm} = 199$ eV. This reduced c.m. plot of $\rho = \theta \sin \theta \frac{d\sigma}{d\omega}$ vs. $\tau = E_{cm} \theta$ has the threshold behavior characteristic of an inelastic process occurring on a repulsive wall⁴⁻⁶ and contrasts markedly with the apparent lack of an inelastic threshold seen in the ρ - τ plots for feature A (Fig. 5). Defining the threshold τ_t as the τ value corresponding to half the peak value, one obtains from Figure 6 a threshold of $\tau_t \approx 725 \pm 25$ eV-degrees for feature C. The result is the same at $E_{cm} = 99$ eV.

Since feature B first appears at small angles as a shoulder on peak A, its angular dependence is difficult to determine. The rapid decrease in its intensity $\frac{d\sigma}{d\Omega}$ as it shifts to larger ΔE values at larger angles suggests that its angular dependence is qualitatively similar to that of feature A, but no ρ - τ angular threshold can be determined.

Feature D is only observed at small angles, disappearing above $\tau = 600$ eV-deg, although it could be masked by the shifting of feature B toward and through the same energy loss values. A c.m. angular distribution for an energy loss of 19 eV (corresponding to peak D) is shown in Fig. 7 at $E_{\text{cm}} = 99$ eV. The measured threshold τ_t is $\sim 310 \pm 15$ eV-deg and the distribution peaks near $\tau = 450 \pm 40$ eV-deg. Beyond 600 eV-deg the intensity increase is due to the shifting of peak B to higher energy loss values.

At $\theta_{\text{lab}} \geq 10^\circ$, where the intensity was too small for detailed double differential cross section measurements with detector B, supplementary measurements of angular distributions $\frac{d\sigma}{d\Omega}$ were made with detector A. Although these measurements cannot yield detailed information on the product c.m. distribution, they are still useful for estimating the fraction of the total ionization cross section scattered at $\theta_{\text{cm}} \geq 20^\circ$ ($\theta_{\text{lab}} \geq 10^\circ$ for forward scattered ions). This is the fraction of the total cross section that has not been examined by energy analysis. At $E_{\text{cm}} = 200$ eV this fraction is estimated to be less than 30% of the total cross section. At higher energy the distribution is even more strongly peaked at small angles.

Background due to ground state He in beam

The effect of reaction (3) can be examined most readily by replacing the mixed metastable-ground state beam by a beam of pure ground state He. The He beam ($E_0 = 398$ eV) was produced by resonant charge transfer in a

charge exchange cell filled with He gas and scattered and detected under identical conditions to those for the metastable beam. Two energy profiles for reaction (3) are included in Fig. 4 (panels g and h) for laboratory scattering angles of 5.1° ($\tau = 2030$ eV-degrees) and 9.0° ($\tau = 3600$ eV-degrees). The normalization of the results to the mixed metastable-ground state beam used in Fig. 4 is based on an estimated He/He^* ratio of 2:1 in the metastable beam.⁹ The shape of this distribution is quite comparable to profiles obtained by Brenot et al.⁵ under similar conditions.

Clearly the ground state contribution at 9° (3600 eV-deg) is quite substantial for large values of ΔE . The contribution at 5.1° ($\tau = 2030$ eV-degrees) is small (certainly less than 10% at all values of ΔE), and at even smaller angles it is negligible. The data at lower energies (Figs. 2 and 3) are all at τ values low enough to be virtually unaffected by contributions from collisional ionization of ground state He in the beam. The uncertainty due to ground state contributions beyond ~ 3000 eV-degrees suggests caution in drawing any conclusions from the scattering results at large τ values.

Other possible beam contaminants

Since there is no mass selection for the primary ion beam, concern arose over the possibility of a small contaminant beam component yielding significant intensity of product ions. For example, a small leak of N_2 into the source would yield an N_2^+ component in the ion beam (perhaps

enhanced in intensity due to Penning reactions in the ion source); near-resonant charge transfer of N_2^+ with Cs would produce $N_2(C^3\Pi_u)$ and radiation cascade would yield a mixture of $N_2^*(B^3\Pi_g)$ and $N_2^*(A^3\Sigma_u^+)$. These could be collisionally ionized in the scattering cell and N_2^+ would be detected along with the true He^+ signal. To eliminate the possibility of any such contaminants, a TOF experiment was performed using the same pulsing method applied to the beam energy determination. In this case, however, the flight time was measured from the pulser through the 127° analyzer to detector B. Since mass 4 (He^+) is so far removed from any of the possible contaminant masses, its flight time was easy to resolve and identify. This method of simultaneously determining the velocity and energy of an ion was used to verify that each of the four major ionization features (A,B,C,D) was due to mass 4 (He^+); no significant contamination of the results with other masses was observed.

Other ionic products

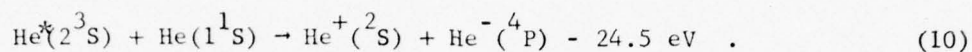
The associative ionization reaction



is less endothermic than reactions (1) and (2) and might contribute to the reaction cross section at low energies. However, at the energies considered here, the electron must remove considerable energy to stabilize the product ion; and associative ionization is unlikely. Since the He_2^+ product ions are expected to have "exactly" the velocity of the center of mass, one can collect any products efficiently at an analysis energy of

half the incident beam energy and an angle of 0° . We could detect no evidence of associative ionization in these experiments.

Another possible reaction produces the stable $\text{He}^- (1s2s2p)^4 \text{P ion}^{12}$ through



The energy loss of 24.5 eV confines any fast He^- (i.e., He^- produced in the forward direction corresponding to slow He^+ product) to a specific velocity at every scattering angle. With a 398 eV He^* beam a search for He^- was made but no convincing evidence of its presence was obtained. We concluded that reaction (10) could contribute no more than a very small fraction of the He^+ signal seen at $\Delta E \approx 25 \text{ eV}$.

DISCUSSION

As mentioned previously, we will initially concentrate our attention on $\text{He}(2^3\text{S})$ because it is predicted to be a much larger fraction of the beam than $\text{He}(2^1\text{S})$; effects possibly due to the $\text{He}(2^1\text{S})$ component will become apparent as we proceed in the discussion.

The interpretation of the $\text{He}(2^3\text{S}) + \text{He}(1^1\text{S})$ collisional ionization data requires not only a knowledge of the potential energy curves for the $\text{He}(2^3\text{S}) + \text{He}$ system, but also a knowledge of the various potential curves for the $\text{He}^+ + \text{He}$ system. In order to understand these processes, we utilize the He_2^* and He_2^+ potential energy curves shown in Fig. 8. The $^3\Sigma_g^+$ adiabatic potential of He_2^* is taken from the work of Lenamon et al.,¹³ and the $^3\Sigma_g^+$ diabatic potential is from the paper by Evans et al.¹⁴ with an exponential extrapolation in the repulsive region. The $^2\Sigma_g^+$ and $^2\Sigma_u^+$ potentials of He_2^+ are from the work of Marchi and Smith¹⁵ with the well depth of the $^2\Sigma_u^+$ state increased slightly to agree with the more accurate results of Liu.¹⁶ The $^2\Sigma_g^+$ potential curve of $\text{He}^+ + \text{He}(2^3\text{S})$ is obtained from an analysis of inelastic scattering data.¹⁷

Given this available potential energy curve information,¹⁸ we can calculate the deflection functions¹⁹ for several possible mechanisms for each ionization process observed experimentally. Then, by comparing the observed and calculated angular thresholds, energy losses, and cross

section behavior, we can appraise the success of various proposed mechanisms at reproducing the experimental results.

We will divide the theoretical interpretation into several parts, each of which is concerned with a specific feature of the collisional ionization of $\text{He}(2^3\text{S})^*$.

Process A

The most prominent ionization mechanism yields a peak of high intensity found at a ΔE of approximately 5 eV associated with ground state ion products and very low energy electrons. This peak has an extremely large intensity and more surprisingly, is found at very small scattering angles, peaking at 0° . If there is an angular threshold in the ρ - τ plots (Fig. 5), it must be at τ values below 100 eV-degrees.

We have calculated the deflection functions for two possible paths that can lead to an energy loss of approximately 5 eV. One possibility is for the particles to follow the adiabatic $^3\Sigma_g^+$ potential and then transfer to the $^2\Sigma_u^+$ potential of He_2^+ on the repulsive walls of the potentials with ejection of a very low energy electron, $E_e \lesssim 1$ eV. Another mechanism involves the small percentage of the $\text{He}(2^3\text{S})^* + \text{He}$ collisions which follow the diabatic $^3\Sigma_g^+$ potential and emit a low energy electron upon crossing into the $\text{He}_2^+ + e$ continuum. We have shown¹ that an ionization mechanism based on the adiabatic approach would yield an ionization threshold at approximately 700 eV-deg, and no scattering at small angles, in complete disagreement with the experimental results.

Although half of the incident $\text{He}^*(2^3\text{S})$ follows the adiabatic $^3\Sigma_u^+$ potential not considered here, any ionization from this less repulsive curve must occur at much smaller R and yield a threshold angle even further from the experimental result. In contrast, the diabatic approach mechanism, whose deflection function is shown in Fig. 9, leads to a considerable amount of scattering near 0° . The reason for this is the large range of impact parameters ($b \approx 1.7 - 2.8 a_0$) contributing to the small angle scattering as seen in Fig. 9, and the fact that the intensity at small angles is further accentuated by an inelastic rainbow effect due to the minimum on the diabatic deflection function. The attractive forces on the $^2\Sigma_u^+$ ion curve essentially compensate for the repulsive forces on the incoming diabatic state, resulting in small overall deflection angles. Hence, it appears that the dominant ionization mechanism occurs through a diabatic channel.

We can estimate the percentage of the particles that follow the diabatic $^3\Sigma_g^+$ potential into the continuum by using the transition probabilities calculated by Evans et al.¹⁴ for the reaction $\text{He}^*(2^3\text{S}) + \text{He} \rightarrow \text{He}(2^3\text{P}) + \text{He}$. This is a single transition from the lowest to the next highest adiabatic $^3\Sigma_g^+$ potential curve. Following the diabatic $^3\Sigma_g^+$ potential into the continuum can be viewed as involving a series of such transitions between successively higher and closer-spaced adiabatic curves. The spacing between the first two adiabatic curves is much larger than the other spacings, implying that the transition probability into the continuum is not very different

from the value for this first crossing. The close-coupled transition probabilities of Evans et al.¹⁴ can be used to obtain the jumping probability from 2^3S to 2^3P in a single crossing of the region of mixing. For impact parameters near the inelastic rainbow this probability is a few tenths of a percent at a c.m. collision energy of 50 eV and 2-5% in the energy range from 100 eV to 200 eV. The coupling matrix elements calculated by Cohen²⁰ for the higher crossings can be used in a Landau-Zener treatment to estimate that the overall probability for continuing diabatically into the continuum is ~ 50 -90% of the $2^3S \rightarrow 2^3P$ probabilities in this energy range. Hence, the overall transition probabilities are substantial and increase by approximately an order of magnitude from 50 eV to 200 eV. This is in good qualitative agreement with the estimated experimental energy dependence, obtained from a normalization of product ion signals at the three energies (Fig. 5).

A schematic molecular orbital correlation diagram for He + He collisions is shown in Fig. 10. In a molecular orbital picture²¹ the diabatic $^3\Sigma_g^+$ state has $1s\sigma_g^2 2p\sigma_u^2 2s\sigma_g$ character at small R and the ionization involves a two electron transition to the ionic state $1s\sigma_g^2 2p\sigma_u$ and a free electron. One electron drops down to fill the vacancy in the lowest molecular orbital while another is promoted into the continuum.

The small component of He $^*(2^1S)$ in the beam has an analogous diabatic $^1\Sigma_g^+$ path into the continuum. The diabatic $^1\Sigma_g^+$ potential and the

low-lying adiabatic $^1\Sigma_g^+$ potentials have been calculated by Guberman and Goddard.²² The major relevant difference between the $^1\Sigma_g^+$ and $^3\Sigma_g^+$ potentials for a comparison of overall probabilities for proceeding diabatically into the continuum involves a smaller splitting in the $^1\Sigma_g^+$ case between the incoming (2^1S) and the next highest (2^1P) adiabatic curve. Close-coupled transition probabilities are not available for the $(^1\Sigma_g^+) He^*(2^1S) + He \rightarrow He(2^1P) + He$ excitation; but the smaller splitting²³ implies a much greater transition probability, with a magnitude of roughly 20-50% in the c.m. energy range 50-200 eV.

The ratio of $He^*(2^3S)$ to $He^*(2^1S)$ in the beam is estimated theoretically to be ~ 30 -50 in this energy range.⁹ Comparing the estimated beam ratios and estimated transition probability ratios for the two metastable components of the beam suggests that the contribution of the $He^*(2^1S)$ metastable to the collisional ionization may be substantial, especially at $E_{cm} = 50$ eV where the transition probability along the diabatic $^3\Sigma_g^+$ potential becomes quite small.

Since the beam composition and diabatic transition probabilities are only theoretical estimates with no experimental confirmation, the relative contribution of $He^*(2^1S)$ to the ionization can only be crudely estimated; and there is no easy way to separate the two contributions experimentally. The difference in initial energy of 0.8 eV between the two levels implies that the deflection function for ionization of the $He^*(2^1S)$ should be slightly less repulsive than the calculated result for the 2^3S component (Fig. 9) and that the energy loss values should

be lower by 0.8 eV. It should be noted that as the c.m. energy varies from 50 to 200 eV the measured energy loss of peak A varies from 4.5 ± 0.5 eV to 5.5 ± 0.5 eV, consistent with the suggested decrease in the $\text{He}(2^1\text{S})^*$ contribution with increased energy. However, another effect can be responsible for this shift, an increase in the emitted electron energy with increased collision energy due to quicker transit into the continuum.^{2,3} Other strong evidence for contributions of $\text{He}(2^1\text{S})^*$ to the observed ionization exists in our observation that process D is due entirely²³ to the singlet component of the beam; clearly, the $\text{He}(2^1\text{S})^*$ contribution to other ionization features, including feature A, cannot be discounted.

Our description of process A has so far been limited to a single channel even though other contributions to ionizations with an energy loss of ~ 5 eV are possible. For example, one can follow the diabatic $^3\Sigma_g^+$ (or $^1\Sigma_g^+$) curve all the way to the turning point and ionize on the outgoing trajectory near the crossing out of the continuum. This process involves a larger amount of repulsive interaction and should not contribute to the intense forward scattering. However, if a significant fraction of the incoming flux can reach and return from the inner turning point without suffering autoionization, this channel might contribute to feature A at larger τ values.

Consider further the case where the outgoing flux continued down through the continuum crossing without autoionizing. Since the original probability of

following the diabatic $^3\Sigma_g^+$ curve into the continuum was small, the chance of returning elastically must also be small. This could lead to excitation of excited states lying between the incoming level and the continuum. Among these are excited ionic states of the form $\text{He}^+ + \text{He}^-(1s^2 n\ell)$. Although, to our knowledge, there is no evidence for $\text{He}^-(1s^2 n\ell)$ states, they may exist in the field of a He^+ , yielding potentials that are coulombic at large distances and are asymptotically above the $\text{He}^+ + \text{He}$ continuum. Barat and co-workers^{4,5} have invoked such states to explain similarities in excitation and ionization channels for ground state He-He collisions. If these states are populated on the outgoing leg of the trajectory, they will cross into the continuum at large distances, yielding a low energy electron and contributing to process A. The coulombic attraction can compensate for the earlier repulsion to produce low angle scattering and an inelastic rainbow. Another possibility involves collisions following the adiabatic $^3\Sigma_g^+$ (or $^1\Sigma_g^+$) potential to the turning point, then making a transition (diabatic) to a $\text{He}^+ + \text{He}^-$ potential on the outgoing trajectory. In either case the coulombic exit channel must pass diabatically with little interaction at large distances through a manifold of excited neutral states of the same symmetry if the continuum is to be reached.

In a companion paper, Saxon et al.²³ calculate the lowest $^1\Sigma_g^+$ potential curves of He_2 formed from 1s and 2s electrons. There are two singly excited $^1\Sigma_g^+$ curves associated with $\text{He}^*(2^1S) + \text{He}(1^1S)$ and $\text{He}^+ + \text{He}^-(1s^2 2s, 2^2S)$,

respectively, at large distances. The repulsive diabatic $^1\Sigma_g^+$ potential has the character of the $\text{He}^* + \text{He}$ adiabatic curve at large distances and resembles the $\text{He}^+ + \text{He}^-$ adiabatic potential at smaller R .

At present, evidence for possible contributions to process A from large distance autoionization along a coulombic $\text{He}^+ + \text{He}^-$ potential are rather difficult to separate from the mechanism proposed. Other ionization features discussed below demonstrate directly the importance of the repulsive diabatic potential, whereas evidence of the long-range autoionization comes indirectly from other experimental results on the $\text{He} + \text{He}$ system.^{4,5} The various possible contributions to feature A for each metastable should interfere coherently, and any oscillations, if they were to be observed, could possibly be identified with specific channels. Unfortunately, the oscillation patterns might be washed out, since there are several possible important interfering channels for two different incident metastables.

Process B

One of the most interesting observations is an energy loss that changes with angle and collision energy but is well correlated with the reduced angle $\tau = E\theta$ (see Fig. 11). This implies that the energy loss process depends directly on the impact parameter. The observed energy losses increase with increasing τ and vary from approximately 9 to 20 eV, with values outside this range possibly obscured by overlap with other ionization features. This behavior can be ascribed to a collision in

which the system follows the diabatic incoming channel until it reaches the classical turning point R_0 , ionizes at the turning point, and exits along the ground state ($^2\Sigma_u^+$) He_2^+ potential. Ionization at the turning point is consistent with a classical formulation of ionization within a continuum where the probability of ionization at a given impact parameter b is given by an integral over all internuclear separations²⁴

$$P_{\text{ion}}(b) = 1 - \exp \left(-2 \int_{R_0}^{\infty} \frac{\Gamma(R) dR}{\hbar v_0 (1 - V(R)/E - b^2/R^2)^{1/2}} \right).$$

Since the coupling to the continuum, the width Γ , is divided by the radial velocity before integration, autoionization of the molecular state formed during the collision should have a peak at the distance of closest approach where the radial velocity is zero.

To demonstrate this effect for $\text{He}(2^3S)$ collisions, we calculated a deflection function using the diabatic $^3\Sigma_g^+$ potential and the $^2\Sigma_u^+$ ion potential (similar results would be obtained with incident $\text{He}(2^1S)$ metastables). The result is plotted as τ_B in Fig. 9. Corresponding energy loss values were determined from the potential differences at the turning point and are plotted along with the experimental data for feature B in Fig. 11. The agreement is quite good except at the large τ values corresponding to small R_0 where the potential curves are strongly repulsive. Here the energy loss is strongly dependent on slight changes in the relative slopes of the two curves; since the

calculated curves are essentially parallel, the predicted energy loss values become constant.

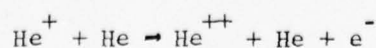
Consideration of the molecular orbital characters of the two relevant potential curves, however, suggests that the "true" potentials continue to separate as the turning point decreases and that the extrapolation of the ${}^3\Sigma_g^+$ diabatic curve at small distances should be higher than shown in Fig. 8. Above the continuum crossing, the ${}^3\Sigma_g^+$ diabatic potential can be characterized by the configuration $1s\sigma_g 2p\sigma_u^2 2s\sigma_g$, while the ground state ${}^2\Sigma_u^+$ ion potential has a $1s\sigma_g^2 2p\sigma_u$ configuration in the same region. The difference potential should be dominated by the extra antibonding $2p\sigma_u$ electron in the ${}^3\Sigma_g^+$ potential and the extra bonding $1s\sigma_g$ electron in the ion curve. Actually, the ${}^3\Sigma_g^+$ diabatic potential should be more nearly parallel at small R to the ${}^2\Sigma_g^+$ ion curve whose configuration $1s\sigma_g 2p\sigma_u^2$ is different only in the relatively small effect of the $2s\sigma_g$ electron. Hence, a better value for the potential at small R should yield an energy loss for process B which continues to increase with τ , in agreement with the experimental data. The ionization process is again a two electron transition from $1s\sigma_g 2p\sigma_u^2 2s\sigma_g$ to $1s\sigma_g^2 2p\sigma_u + e^-$, as indicated schematically in Fig. 10.

The experimental data (Figs. 3, 4) contain strong evidence of secondary structure developing between peaks A and B at large angles (Figs. 3i, 3j, 4d-f). The most convincing evidence is obtained from the similarities in this secondary structure at different energies when they

are compared at the same τ value, e.g., Figs. 3j and 4d. This structure can be understood by considering the consequences of the fact that the ionization does not occur exclusively at the turning point.

All scattered ions from process B found at a specified energy loss ΔE_1 correspond to a single internuclear distance R_1 at which the electron emission occurs. The largest intensity is associated with collisions whose turning point is precisely R_1 , but collisions with smaller impact parameters can ionize at R_1 either on the incoming or the outgoing leg of their trajectories. For the specified energy loss ΔE_1 , one can represent the heavy particle interactions by translating the $^2\Sigma_u^+$ ion curve upwards so that it intersects the incoming diabatic curve at R_1 . Then it is easy to see that interference between ionization on the incoming and outgoing legs of the trajectory yields Stückelberg oscillations in the angular distribution equivalent to those observed in a two-state inelastic scattering problem.²⁵ At other energy loss values the angular distribution will have similar interference structure, but will be shifted in the same way that the angular distribution of feature B shifts with energy (Fig. 11).

This structure in both angle and energy is probably responsible for the secondary oscillations observed in the data. No quantitative analysis of this effect will be attempted since the quality of the data does not warrant it. An analysis by Sidis²⁶ of a similar effect observed by Barat et al.²⁷ for the reaction



demonstrates, however, that the mechanism proposed here is a reasonable way of explaining the structure.

Process D

The combination of small scattering angles coupled with large energy losses (18.7 ± 0.5 eV) for peak D causes some difficulty in producing a reasonable explanation of the process involved. There appears to be no realistic ionization mechanism involving $\text{He}(2^3\text{S})$ that would produce such a result. However, for the $\text{He}(2^1\text{S})$ metastable, radial coupling of the incoming $1\Sigma_g^+$ diabatic state with the doubly excited $1\Sigma_g^+$ state dissociating to $\text{He}(2^3\text{S}) + \text{He}(2^3\text{S})$, followed by molecular autoionization at large distances on the doubly-excited curve, would yield an energy loss of 19.0 eV. Yet, it is not immediately clear why this doubly excited curve would be favored over all the similar higher energy states and why the scattering would be found at such low angles.

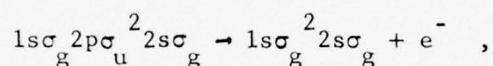
A companion paper²³ presents an ab initio calculation of the relevant $1\Sigma_g^+$ excited He_2 potentials, verifies the existence of a crossing between the incoming diabatic potential and a deep inner well in the doubly excited He_2 potential, and demonstrates that an inelastic rainbow effect can produce low angle scattering into this channel. The crossing from the incoming diabatic potential to the doubly excited $1\Sigma_g^+$ curve involves the two electron transition from $1s\sigma_g 2p\sigma_u$ to $2s\sigma_g$.

$1s\sigma_g^2 2s\sigma_g^2$ (see Fig. 10). The existence of molecular autoionization at large distances on this exit channel potential has already been demonstrated in ground state He-He collisions by Gerber et al.³

Process C

Another prominent inelastic process is characterized by an energy loss of approximately 25-27 eV which has a broad threshold with a half-rise point at $\tau = E\theta \approx 725$ eV-deg. The τ threshold is constant as the collision energy is varied which implies that the mechanism for the production of this channel involves a curve crossing²⁵ (i.e., not rotational coupling in the united atom limit). This energy loss seems consistent with Reaction (2a) and can be readily understood by referring to the potential energy diagram shown in Fig. 8. At small internuclear separations, the diabatic $^3\Sigma_g^+$ potential energy curve of He_2^* approaches the excited ionic $^2\Sigma_g^+$ potential curve arising from $\text{He}^+ + \text{He}(2^3S)$. If in the interaction region labeled C a low energy electron is ejected, an ionization process with an energy loss of ~ 25 eV would be observed (Reaction 2a). It is possible to estimate the angular threshold for this energy loss process from a deflection function analysis. From calculations using the potential curves in Fig. 8, we estimate a threshold of approximately 900 eV-deg. The calculated deflection function is labelled τ_c in Fig. 9. In a discussion of process B above, it was noted that the diabatic $^3\Sigma_g^+$ potential is probably more repulsive at small distances than shown in Fig. 8. This would move the coupling region C to larger R values and should shift the threshold for process C to smaller τ values.

Near the threshold for process C, the energy loss value ΔE is ≈ 25 eV, implying a very low energy for the emitted electron. At scattering angles above the threshold, the energy loss value shifts gradually from 25 eV to ~ 27 -29 eV. There are two obvious possible causes of the shift: ion production accompanied by population of the set of higher neutral states whose asymptotes lie between those of reactions (2a) and (2b); or an increasing energy of the emitted electron accompanying the larger scattering angles. A consideration of the molecular orbitals indicates that excitation of a higher neutral state is unlikely, since reaction (2a) involves the two-electron transition (shown in Fig. 10)



whereas higher excitation must involve additionally a promotion of the $2s\sigma_g$ electron, yielding three-electron transitions of much lower probability.

Another possible contribution to feature C is from excited coulombic states correlating asymptotically to $\text{He}^+ + \text{He}^{-*}$. There is more compelling evidence for the doubly excited He^- states $1sn\ell n' \ell'$ than for the $1s^2 n\ell$ states discussed with relation to feature A. They have been seen as electron scattering resonances,²⁸ and have been utilized in explaining various structure in the electron spectra from He-He collisions.²⁻⁴ From the incoming diabatic state, two-electron transitions can populate molecular orbitals of the form $1s\sigma_g 2s\sigma_g n\sigma$ leading to the possible

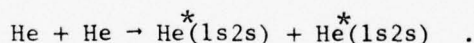
asymptotic population of $\text{He}^+ + \text{He}^-$ ($1s2sn\ell$) states. Autoionization at large distances on these states can produce energy losses compatible with feature C. Coulombic attraction on the outgoing leg of the trajectory could lower the angular threshold for one or more of these $\text{He}^+ + \text{He}^-$ channels below that calculated for Reaction (2a). The best candidate for low angle scattering would involve first a transition to the $1s\sigma_g^2 2s\sigma_g^2$ excited state, followed by a separation along the $\text{He}^+ + \text{He}^-$ ($1s2s^2$) potential rather than the adiabatic $\text{He}^*(1s2s) + \text{He}^*(1s2s)$ curve important to process D. Without ab initio calculations of the $\text{He}^+ + \text{He}^-$ excited potentials it is difficult to assess the importance of these states.

Other Processes

Other ionization channels can open up for smaller impact parameter collisions and larger scattering angles. Examination of a Lichten²¹ type correlation diagram (Fig. 10) demonstrates, for example, the importance of rotational coupling in the united atom limit of the $2p\sigma_u$ and $2p\pi_u$ molecular orbitals. This coupling is important for collisions following the $1,3\Sigma_u^+$ and $1,3\Sigma_g^+$ adiabatic potentials as well as the diabatic curve. The resultant $1s \rightarrow 2p$ transitions can produce $\text{He}(2s2p) + \text{He}$ and higher excitations. Autoionization at large separations of the doubly excited He^{**} states will yield energy losses near ~ 40 eV. Structure at large τ values may be due to this mechanism, but the data are not of sufficient quality to warrant a more detailed examination. Also, contributions from

the ground state component of the beam become important in the same region of τ and energy loss.

It is worth noting that, except for degeneracies in the united atom limit, there are no important contributions to collisional ionization associated with crossings of molecular orbitals. Transitions to excited states at the normally important crossing of the attractive $2s\sigma_g$ orbital with the repulsive $2p\sigma_u$ must involve two-electron transfer to conserve the g or u character of the incoming state; yet the incoming configurations $1s_g^2 2p_u^2 2s_g^2$ ($1,3\Sigma_u^+$), $1s_g^2 2p_u^2 3p_u^2$ ($1,3\Sigma_g^+$ adiabatic), and $1s_g^2 2p_u^2 2s_g^2$ ($1,3\Sigma_g^+$ diabatic) all do not allow this possibility. Two-electron transitions occur at crossings of molecular states or in the continuum, not at crossings of molecular orbitals. This restriction is not in effect for ground state He-He collisions where the $2p\sigma_u^2 \rightarrow 2s\sigma_g^2$ transition²⁻⁴ produces significant excitation, e.g.,



Expected Electron Energy Distributions

Our analysis of the collisional ionization mechanisms can be used to estimate qualitatively the electron energy distribution expected from these reactions. Clearly, the major peak in the electron energy distribution would be from process A with electrons having an energy below ~ 1 eV. Process B and its interference structure would produce a broad continuum of electron energies extending from peak A to higher energies. Feature C would again yield low energy electrons (a few eV or

lower) and possibly a peak at 19.3 eV if autoionization from the $\text{He}^+ + \text{He}^-$ ($1s2s^2$) potential contributes. Feature D would produce ~ 15 eV electrons from the molecular autoionization although the total intensity might be small relative to the intense continuum distribution from process B that underlies it. The $\text{He}(2s2p)$ autoionizing state mentioned briefly would eject an electron with energy near 35 eV.^{2,29}

It must, of course, be emphasized that up to 30% of the total cross section for ion production at $E_{\text{cm}} = 199$ eV occurs with c.m. scattering angles above $\sim 20^\circ$. The lack of detailed differential scattering data at these angles implies that other mechanisms could contribute substantial electron intensities at energies different from those predicted here.

Recently, product electron energy distributions have been measured for this reaction^{10,30} over a similar energy range. Such measurements have inherently higher resolution and can identify some of the highly excited product channels, but there are experimental difficulties associated with detection of the low energy electrons.³⁰

Total Cross Sections

If, as we conclude, ionization occurs predominantly for collisions following the diabatic incoming potential, we can estimate the total cross section for ionization by assuming that all collisions reaching the continuum eventually yield ions. At c.m. collision energies between 100 and 500 eV, we calculate that the total cross section for $\text{He}^*(2^3S)$ ionization ranges from 1 to $3 \times 10^{-7} \text{ cm}^2$;

it should be significantly larger for $\text{He}^*(2^1\text{S})$ at these energies. At very high energies where almost 100% of the particles would be following the diabatic potential, the cross section becomes

$$\sigma_{\text{ion}} = \frac{1}{2}\pi R_x^2,$$

where the $\frac{1}{2}$ factor comes from the fact that only 50% of the $\text{He}(2^3\text{S}) + \text{He}$ particles follow the gerade potential curve, and R_x is the distance where the diabatic potential crosses into the $\text{He}_2^+ + e$ continuum. Since $R_x \approx 2.8 a_0$, we obtain a high energy result for σ_{ion} of $3.4 \times 10^{-16} \text{ cm}^2$, which is in extremely good agreement with the measurements of Gilbody et al.³¹ in the c.m. energy range 15-175 keV.

To assess the contribution of collisional ionization to the destruction of fast metastable He in collisions with He target, we can compare these estimates of the ionization cross section with measured³² total destruction cross sections σ_d . In the c.m. energy range 500 to 1100 eV, σ_d is $\sim 5 \times 10^{-16} \text{ cm}^2$ for $\text{He}^*(2^3\text{S})$ and $\sim 8 \times 10^{-16} \text{ cm}^2$ for $\text{He}^*(2^1\text{S})$, implying that ionization channels can account for a significant fraction of σ_d at keV energies.

Summary

We have discussed various mechanisms for collisional ionization in $\text{He}^* + \text{He}$ collisions and their relationship to the experimental He^+ distributions. Most of the structure can be understood in terms of a few ionization mechanisms involving an incoming repulsive diabatic potential.

In the most prominent process the electron is ejected as the initial diabatic potential curve crosses into the continuum. Further ionization is found to occur near the distance of closest approach (as occurs in Penning ionization), and at crossings with higher continua. Contributions from coulombic $\text{He}^+ + \text{He}^-$ states leading to long-range autoionization of He^- are also possible. At high energies and small impact parameters, transitions to autoionizing neutral He^{**} states are also expected. Even though most collisions occur along the $1,3\Sigma_u^+$ or $1,3\Sigma_g^+$ adiabatic potentials, the major contribution to ionization comes from those proceeding diabatically into the continuum. Significant contributions to ionization from the 2^1S metastable seem likely, even though it is expected to be a minor component of the beam.

ACKNOWLEDGEMENT

We appreciate Dr. R. Morgenstern making available to us a preview of the electron energy distribution measurements from Freiburg.

KTG acknowledges helpful conversations with Drs. M. Barat, D. L. Huestis, D. C. Lorents, R. P. Saxon, and A. Salin regarding this work.

REFERENCES

[†]This research was supported by the Office of Naval Research under Contracts N00014-70-C-0339 and N00014-76-C-0118.

1. K. T. Gillen, D. C. Lorents, R. E. Olson, and J. R. Peterson, J. Phys. B.: Atom. Mol. Phys. 7, L327 (1974).
2. G. Gerber, R. Morgenstern, and A. Niehaus, J. Phys. B.: Atom Mol. Phys. 6, 493 (1973).
3. G. Gerber and A. Niehaus, J. Phys. B.: Atom. Mol. Phys. 9, 123 (1976).
4. M. Barat, D. Dhuicq, R. Francois, C. Lesech, and R. McCarroll, J. Phys. B.: Atom. Mol. Phys. 6, 1206 (1973).
5. J. C. Brenot, D. Dhuicq, J. P. Gauyacq, J. Pommier, V. Sidis, M. Barat, and E. Pollack, Phys. Rev. A 11, 1245 (1975).
6. J. C. Brenot, D. Dhuicq, J. P. Gauyacq, J. Pommier, V. Sidis, M. Barat, and E. Pollack, Phys. Rev. A 11, 1933 (1975).
7. F. J. Eriksen, S. M. Fernandez, A. B. Bray, and E. Pollack, Phys. Rev. A 11, 1239 (1975).
8. R. Morgenstern, D. C. Lorents, J. R. Peterson, and R. E. Olson, Phys. Rev. A 8, 2372 (1973).
9. R. E. Olson, E. J. Shipsey, and J. C. Browne (unpublished).
10. G. H. Lantschner, Thesis, Freiburg (1975).
11. M. L. Coleman, R. Hammond, and J. W. Dubrin, Chem. Phys. Letters 19, 271 (1973).

12. E. Holoien and J. Midtdal, Proc. Phys. Soc. A68, 815 (1955).
13. L. Lenamon, J. C. Browne, and R. E. Olson, Phys. Rev. A 8, 2380 (1973).
14. S. A. Evans, J. S. Cohen, and N. F. Lane, Phys. Rev. A 4, 2235 (1971).
15. R. P. Marchi and F. T. Smith, Phys. Rev. 139, A1025 (1965).
16. B. Liu, Phys. Rev. Letters 27, 1251 (1971).
17. R. E. Olson, Phys. Rev. A 5, 2094 (1972).
18. See also M. L. Ginter and R. Battino, J. Chem. Phys. 52, 4469 (1970);
W. J. Steets and N. F. Lane, Phys. Rev. A 11, 1994 (1975); and Ref. 20.
19. R. E. Olson and F. T. Smith, Phys. Rev. A 3, 1607 (1971).
20. J. S. Cohen, Phys. Rev. A 13, 86 (1976).
21. W. Lichten, Phys. Rev. 164, 131 (1967); M. Barat and W. Lichten,
Phys. Rev. A 6, 211 (1972).
22. S. L. Guberman and W. A. Goddard III, Phys. Rev. A 12, 1203 (1975).
23. R. P. Saxon, K. T. Gillen, and B. Liu, Phys. Rev. A (following paper).
24. W. H. Miller, J. Chem. Phys. 52, 3563 (1970).
25. See, for example, review by M. Barat, Invited Lectures and Progress
Reports VII ICPEAC, Beograd, 1973, p. 43.
26. V. Sidis, J. Phys. B.: Atom. Mol. Phys. 6, 1188 (1973).
27. M. Barat, D. Dhuicq, F. Francois, R. McCarroll, R. D. Piacentini,
and A. Salin, J. Phys. B.: Atom. Mol. Phys. 5, 1343 (1972).
28. G. J. Schulz, Rev. Mod. Phys. 45, 378 (1973).
29. R. P. Madden and K. Codling, Astrophys. J. 141, 364 (1965).
30. R. Morgenstern, Freiburg (private communication).

31. H. B. Gilbody, K. F. Dunn, R. Browning, and C. J. Latimer, J. Phys. B.: Atom. Mol. Phys. 3, 1105 (1970).
32. M. Hollstein, J. R. Sheridan, J. R. Peterson, and D. C. Lorents, Phys. Rev. A 187, 118 (1969).

FIGURE LEGENDS

- Fig. 1 Kinematic diagram. A beam of He^* of laboratory energy E_0 (velocity v_0) is shown colliding with a He target at rest. Laboratory velocities (v_0, v_c, v') are measured relative to the point O. $v_c (=0.5 v_0)$ is the velocity of the c.m. Velocities in the c.m. system (w, w') are measured relative to the point C. Primed velocities and energies refer to the product particles. Measurement of E' and θ_L for He^+ specifies w', θ_{cm} , and ΔE (see text).
- Fig. 2 Distribution of He^+ ions plotted vs product laboratory energy E' for 0.0° scattering of a 100.2 eV He^* beam by He. The c.m. collision energy is 50.1 eV; several values of the c.m. endothermicity ΔE are indicated.
- Fig. 3 Representative He^+ product laboratory energy distributions for $\text{He}^* + \text{He}$ collisions at a c.m. collision energy of 99 eV. Each spectrum is labelled with the incident beam energy and laboratory scattering angle. All differential cross sections are normalized arbitrarily to unity at the peak of the distribution at 0° using angular normalization data to compare the different angles. Representative values of the c.m. endothermicity ΔE are indicated for each spectrum; the letters A, B, C, D refer to the ionization features described in the text.

Fig. 4 Representative He^+ product laboratory energy distributions for $\text{He}^* + \text{He}$ collisions at a c.m. collision energy of 199 eV. See legend for Fig. 3. The triangular data points in panels g and h present estimates of the He^+ produced from ionization of the ground state component of the beam ; contributions from this channel are insignificant for the other angles shown.

Fig. 5 Experimental angular distributions of the He^+ ions from Feature A at an energy loss of ~ 5 eV. Plotted are the differential cross section $\frac{d\sigma}{d\Omega}$ and the reduced cross sections $\rho = \frac{\theta_L \sin \theta_L}{\theta_L} \frac{d\sigma}{d\Omega}$ vs the reduced angle $\tau = E_0 \frac{\theta_L}{\theta_L}$ in the laboratory. The analogous c.m. cross sections differ insignificantly. The c.m. energy is indicated for each curve. The intensity units are arbitrary, but the relative intensities for the three energies are approximate values obtained from comparing the ion signal to the beam intensity at each of the energies.

Fig. 6 ρ - τ plot in the c.m. of the experimental angular distribution of the He^+ ions from feature C at $E_{\text{cm}} = 199$ eV. Data points in two directions from the He^* beam are indicated by the symbols $+\theta$ and $-\theta$.

Fig. 7 ρ - τ plot in the c.m. of the experimental angular distribution of He^+ ions at $\Delta E = 19$ for $E_{\text{cm}} = 99$ eV. Feature D appears at small τ values; beyond ~ 600 eV-degrees, other processes contribute at this ΔE value.

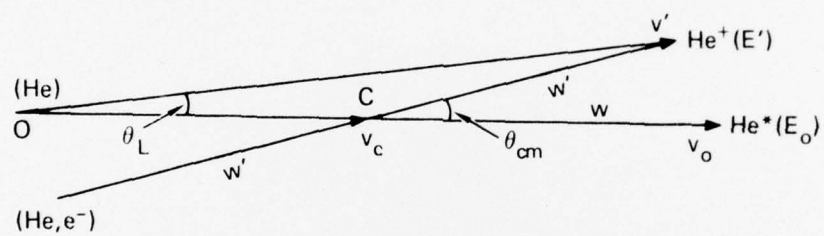
Fig. 8 Several of the He_2^* and He_2^+ potential curves useful for a description of ionization in $\text{He}(2^3\text{S}) + \text{He}$ collisions. Sources for curves: adiabatic $^3\Sigma_g^+$ from Lenamon et al. (Ref. 13); diabatic $^3\Sigma_g^+$ from Evans et al. (Ref. 14) with an exponential extrapolation at small R; $^2\Sigma_u^+$ and repulsive $^2\Sigma_g^+$ from Marchi and Smith (Ref. 15) with the well depth adjusted to Liu's value (Ref. 16); and upper $^2\Sigma_g^+$ from Olson (Ref. 17). The $^3\Sigma_u^+$ curve correlating asymptotically to $\text{He}(2^3\text{S}) + \text{He}(1^1\text{S})$ is not shown; half of the incoming $\text{He}(2^3\text{S})$ metastables follow this potential.

Fig. 9 Deflection functions vs impact parameter calculated for collisions following the $^3\Sigma_g^+$ diabatic potential shown in Fig. 8. For τ_A , ionization occurs at the first crossing into the continuum at point A in Fig. 8; τ_B is the deflection function obtained when ionization occurs at the classical turning point and the products separate on the ground state ion curve; τ_C is calculated assuming transfer to the excited $^2\Sigma_g^+$ ion curve in region C of Fig. 8.

Fig. 10 Molecular orbital correlation diagram for $\text{Be} \rightleftharpoons \text{He} + \text{He}$ showing schematically the lowest orbitals. The orbitals are labelled in united atom nomenclature. The circled arrows at the right represent the electrons in the configuration $1s\sigma_g 2p\sigma_u^2 2s\sigma_g$ corresponding to the incoming diabatic $^3\Sigma_g^+$ molecular potential. The singlet case is similar. The vertical arrows labelled A, B, D, and C show the two-electron transitions associated with

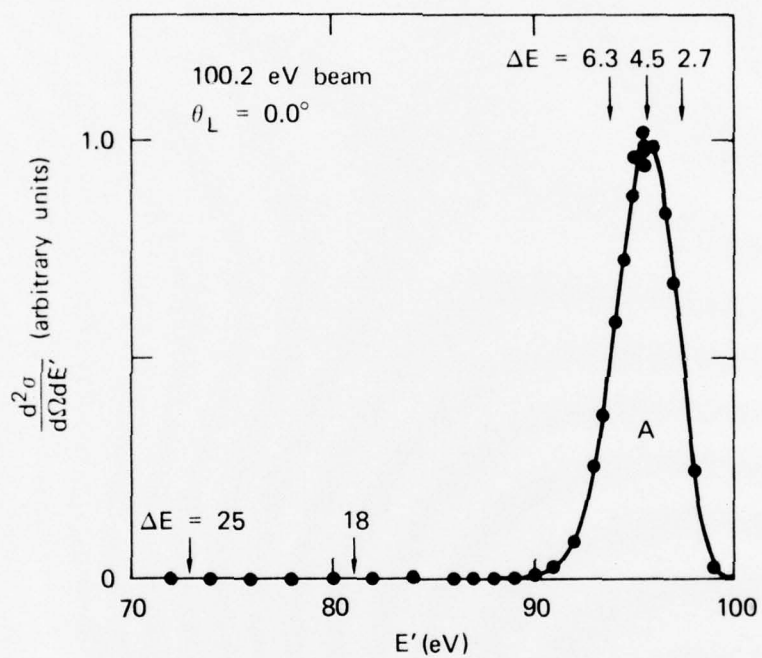
the processes described in the text. Process D is not possible for the triplet component of the beam, but is observed for singlet metastables approaching along the diabatic $^1\Sigma_g^+$ potential; the transition $1s\sigma_g \quad 2p\sigma_u^2 \quad 2s\sigma_g \rightarrow 1s\sigma_g^2 \quad 2s\sigma_g^2$ is followed by ionization at large distances.

Fig. 11 Experimental energy loss values for ionization features A and B plotted vs τ . A theoretical curve for process B is shown which assumes ionization at the turning point on the diabatic curve shown in Fig. 8. Note change of scale at high τ values.



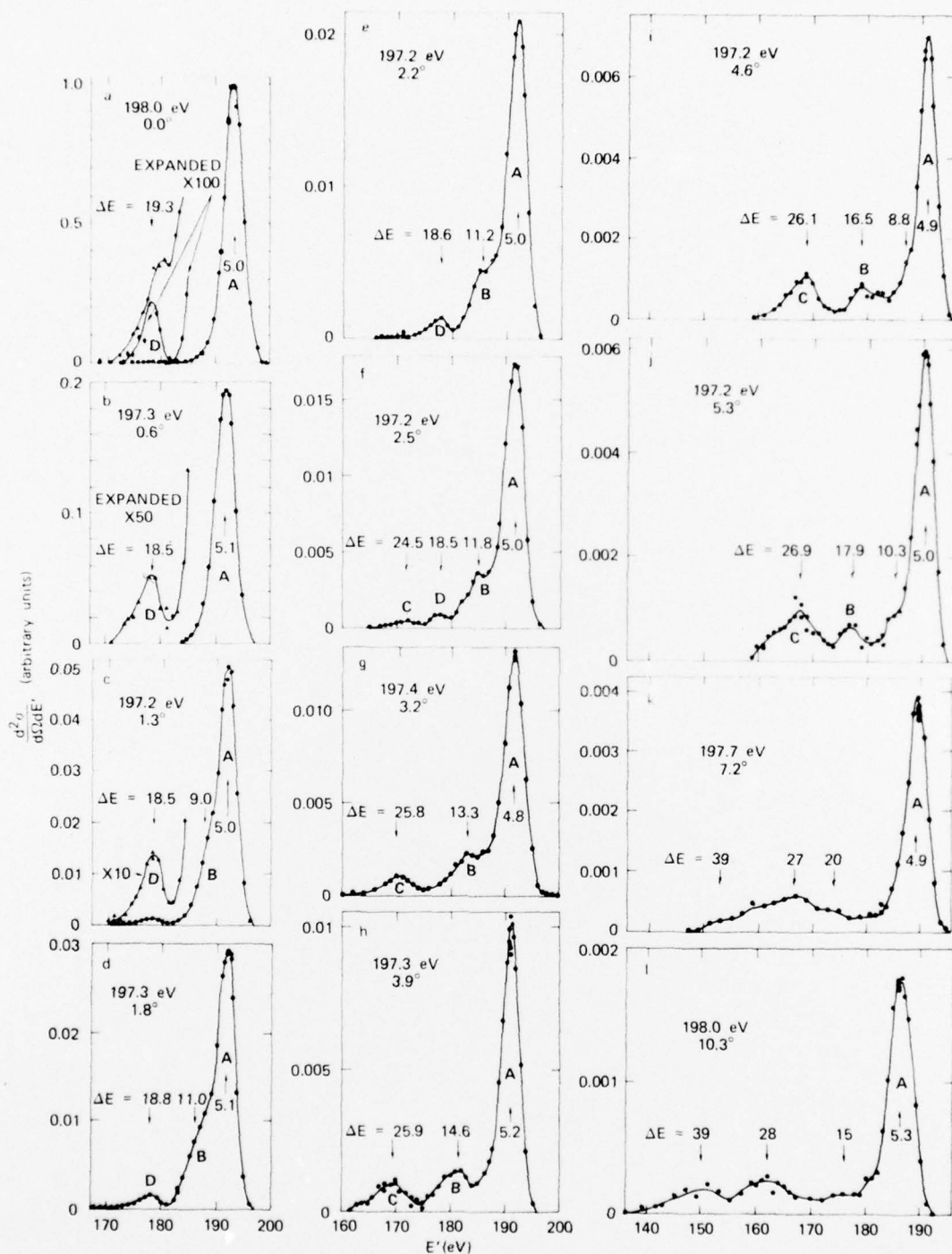
SA-4529-1

FIGURE 1



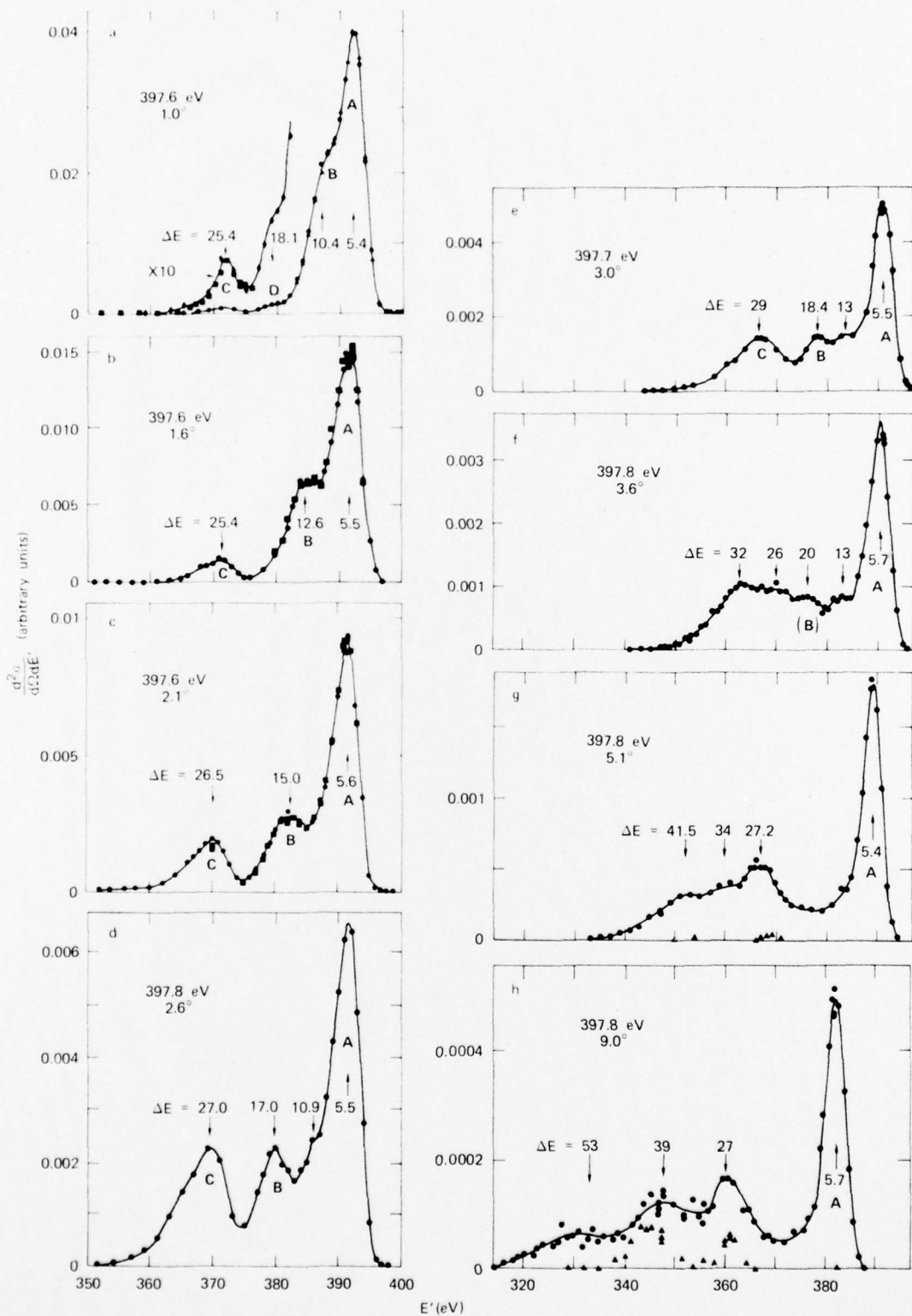
SA-4529-2

FIGURE 2



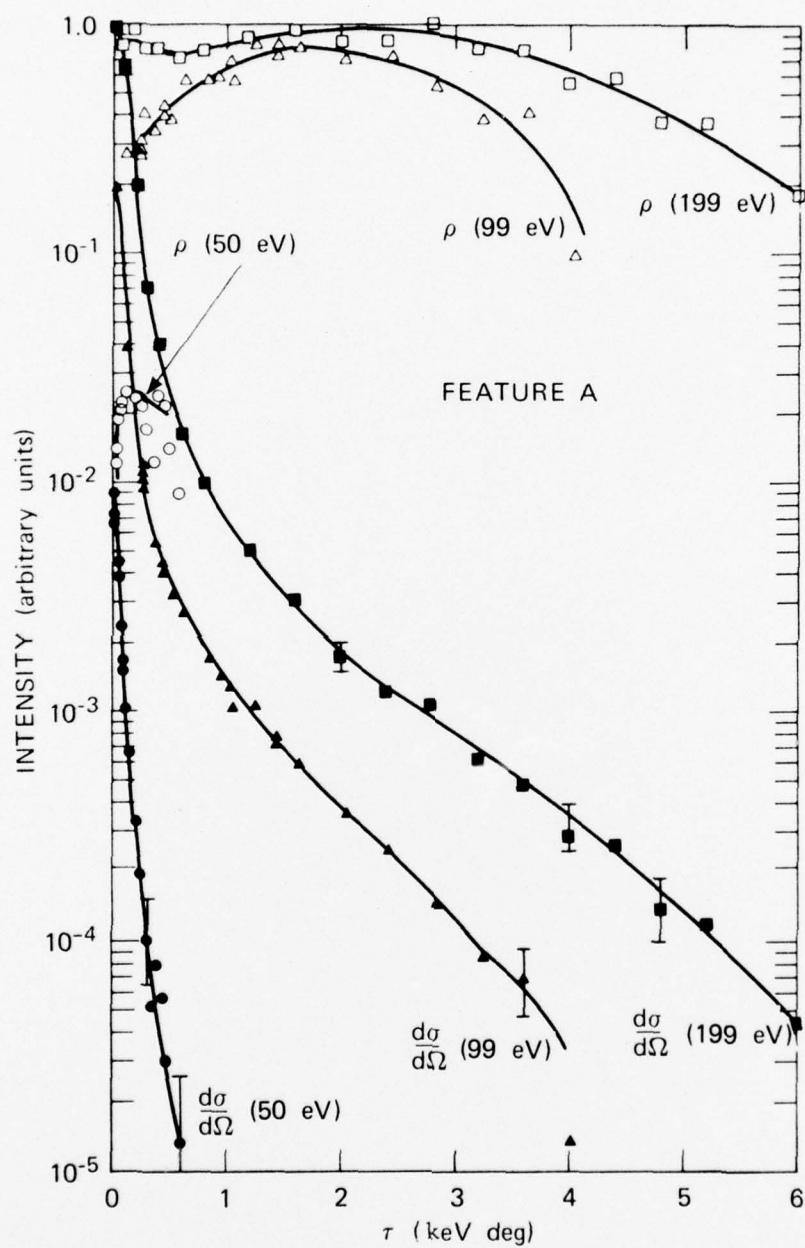
TA-8658-34R

FIGURE 3



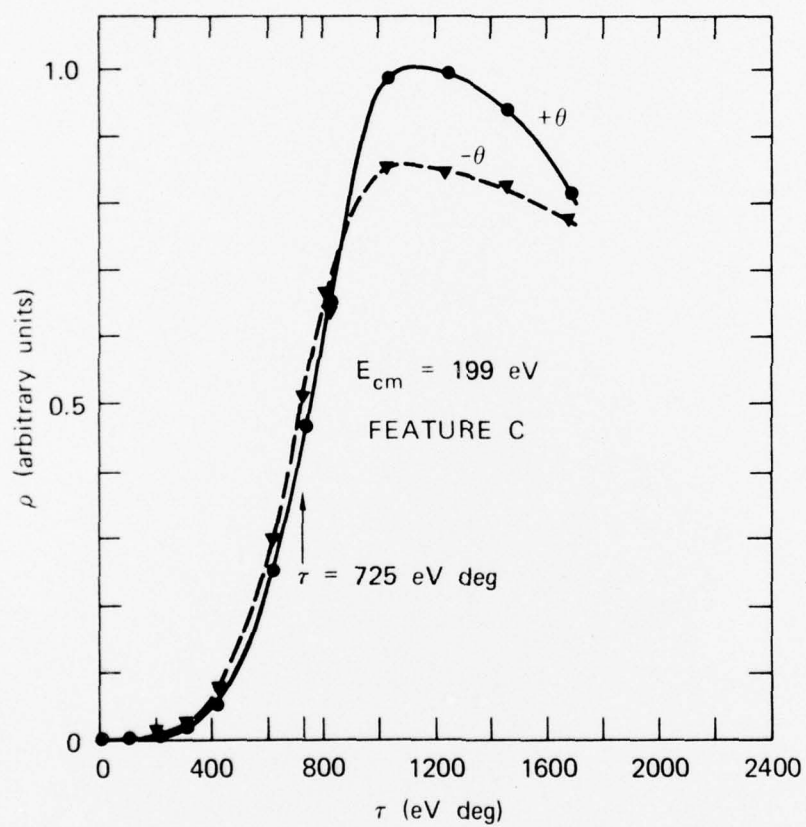
TA-865R-35R

FIGURE 4



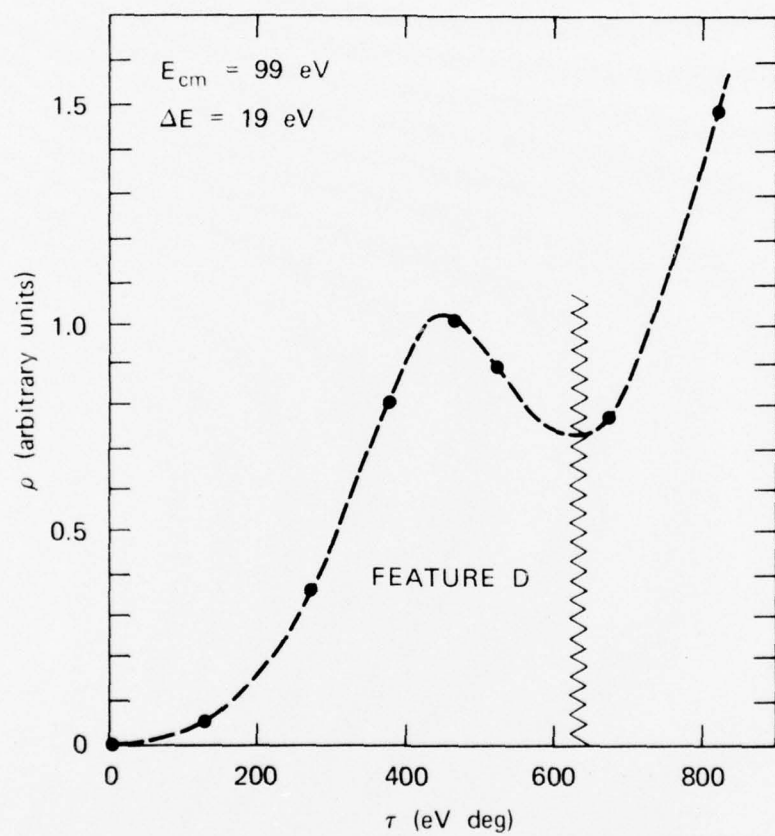
SA-4529-6R

FIGURE 5



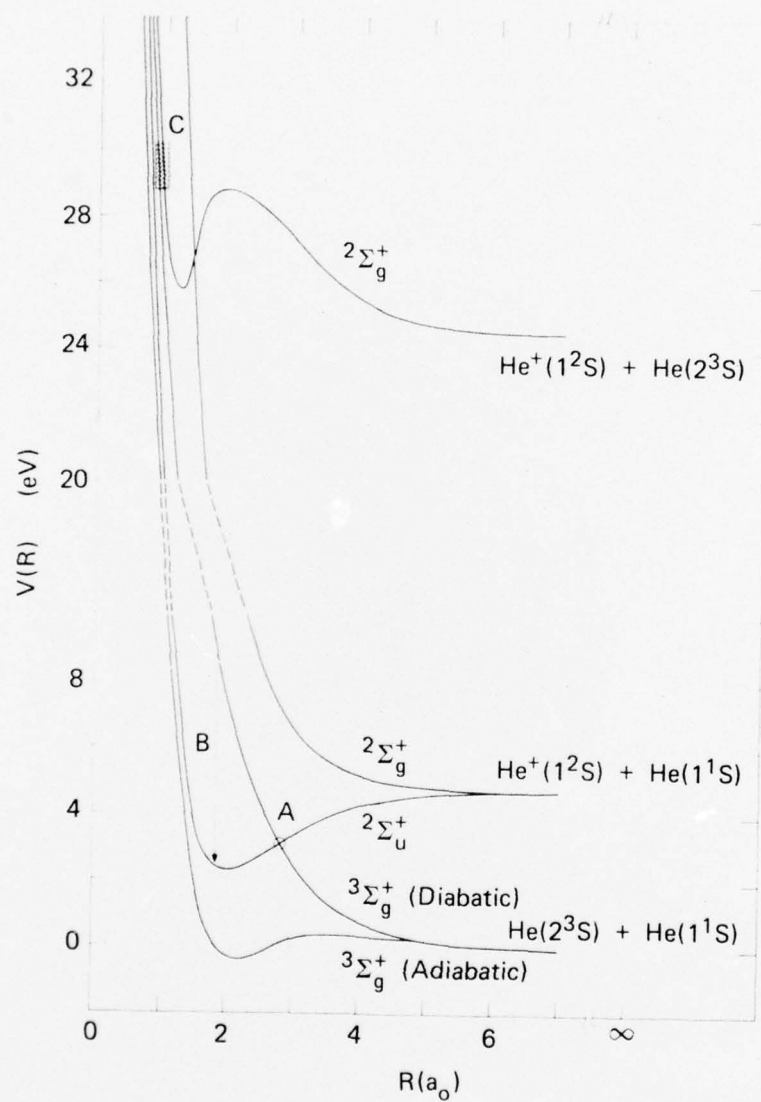
SA-4529-4R1

FIGURE 6



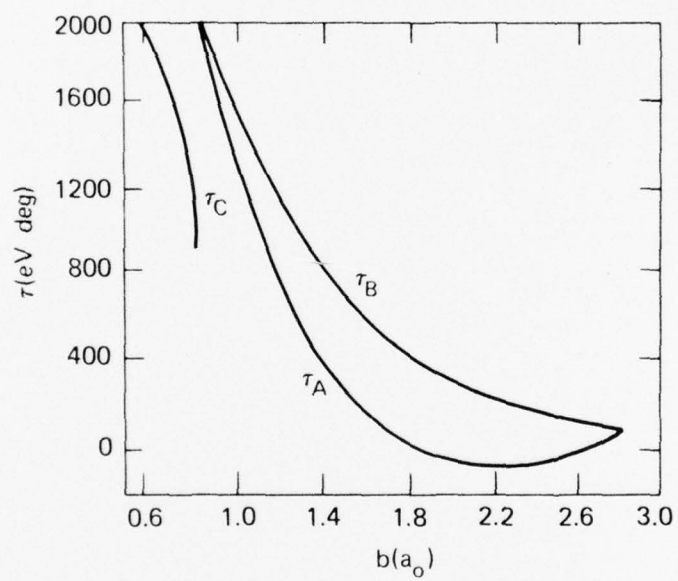
SA-4529-3R1

FIGURE 7



SA-8658-33

FIGURE 8



SA-8658-32

FIGURE 9

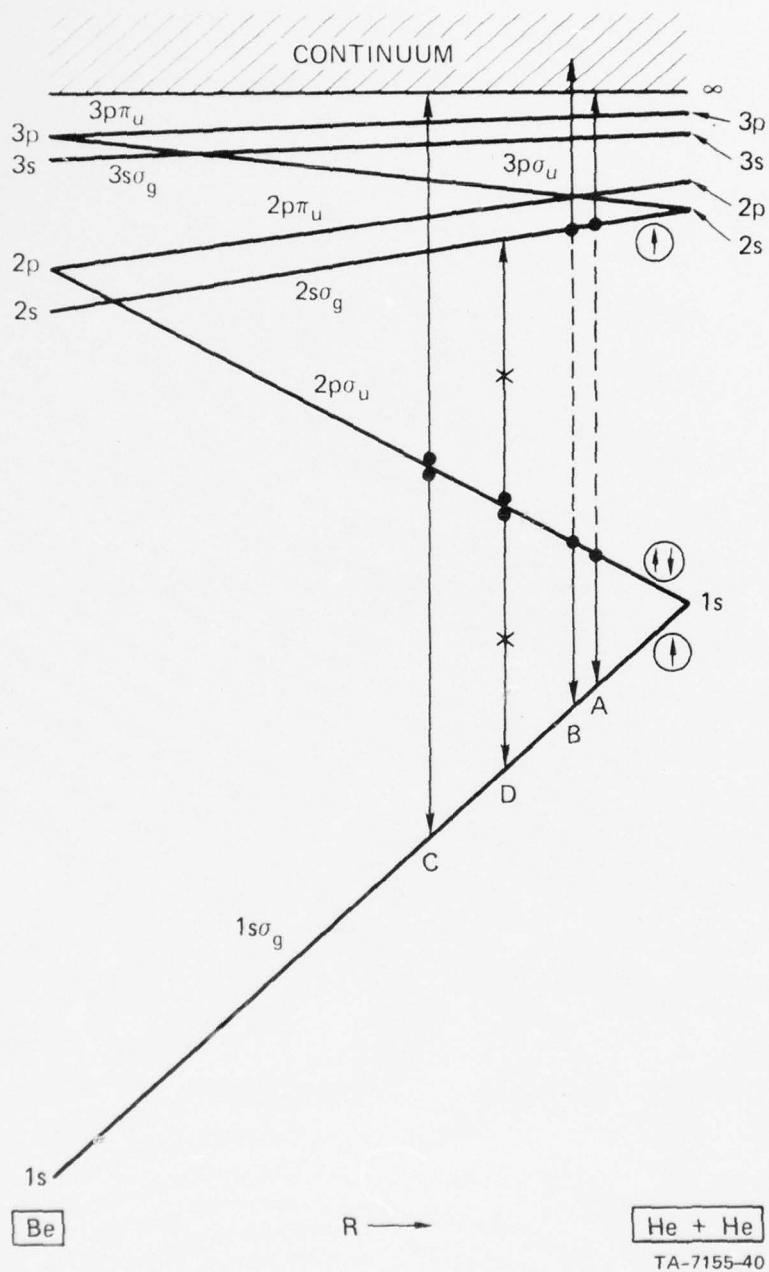
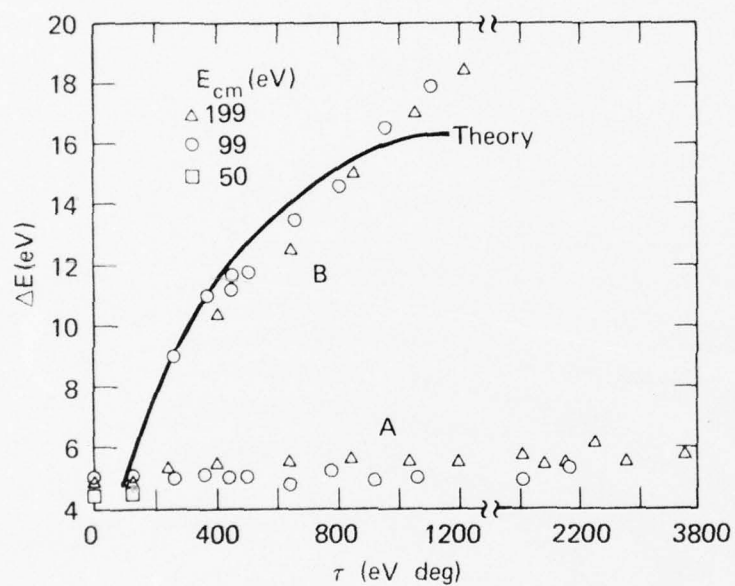


FIGURE 10



SA-4529-5R1

FIGURE 11